THE UNIVERSITY OF MANITOBA

DEVELOPING TURBULENT PIPE FLOW

by

Jack William Richman

A THESIS

SUBMITTED TO THE UNIVERSITY OF MANITOBA

IN PARTIAL FULFILMENT OF THE REQUIREMENTS FOR THE DEGREE

OF DOCTOR OF PHILOSOPHY

DEPARTMENT OF MECHANICAL ENGINEERING

WINNIPEG, MANITOBA

April 1974

DEVELOPING TURBULENT PIPE FLOW

by

Jack William Richman

A dissertation submitted to the Faculty of Graduate Studies of the University of Manitoba in partial fulfillment of the requirements of the degree of

DOCTOR OF PHILOSOPHY

ABSTRACT

The structure of steady axi-symmetric incompressible developing turbulent pipe flow is investigated through quantitative measurements of its mean velocity, stress fields and component energy spectra, for pipe Reynolds numbers of 1×10^5, 2×10^5 and 3×10^5, using air as a working fluid. The measured characteristics are used to evaluate the terms appearing in the time-averaged energy equation to determine energy budgets for the flow. The results illustrate the manner in which the flow adjusts from a boundary layer structure to a fully developed flow structure downstream by virtue of the mixing which occurs when the boundary layer fills the whole of the pipe. It is shown that in the mixing region the pipe centre-line velocity becomes moderately peaked, and then subsides to a velocity characteristic of a fully developed flow. The energy budgets and spectral measurements indicate that the main energy process involved in the mixing region is due to convective diffusion of turbulence energy.

An approximate numerical analysis using an effective viscosity model based on the law of the wall was developed to simulate the flow characteristics of the mean axial and radial velocities, mean vorticity, local wall shear stress and Reynolds shear stress. Comparison of the numerical solutions with the measured data gave reasonably good agree-

ment over the whole flow field, but the effective viscosity model does not yield the centre-line velocity peak in the mixing region.

ACKNOWLEDGEMENTS

The author would like to express thanks to Dr. R.S. Azad for his encouragement and guidance as a research adviser, to Drs. J. Tinkler, K.R. McLachlan and H. Tennekes for their many helpful comments and review of the thesis, and to the National Research Council of Canada, whose financial support made this work possible.

TABLE OF CONTENTS

Page

LIST OF TABLES

LIST OF FIGURES

Figure Page

NOMENCLATURE

A'_J	coefficient in modified general substitution formula
A_E, A_W, A_N, A_S	coefficients in convection terms of difference equation
a	coefficient in general elliptic equation
B'_J	coefficient in modified general substitution formula
B_E, B_W, B_N, B_S	coefficients in diffusion terms of difference equation
b	coefficient in general elliptic equation
C_E, C_W, C_N, C_S	coefficients in general substitution formula
$C_{uv}(\chi)$	coincident spectral density function
C	constant in law of wall equation
D	pipe diameter
d	coefficient in general elliptic equation

$E_{u^2}(\chi)$, $E_{v^2}(\chi)$, $E_{w^2}(\chi)$, $E_{uv}(\chi)$	axial, radial, circumferential and shear spectral densities, non-dimensionalised by $\upsilon^2\eta$
K	one-dimensional wave-number
k	constant in law of wall equation
L	assumed inlet length (=100D)
P	mean static pressure
p	fluctuating static pressure
Q	total pressure
Q_e	total pressure of entering flow at pipe centre-line
$Q_{uv}(\chi)$	quadrature spectral density function
$\overline{q^2}$	mean value of twice turbulent kinetic energy
R	internal pipe radius
Re	pipe Reynolds number
R_s	residual
r	radial cylindrical polar coordinate
S	source term
U	mean axial velocity
U_b	bulk flow velocity
U^+	defined by U/u_*
u	fluctuating axial velocity component
$\tilde{u}$	root mean square value of fluctuating velocity
$\overline{u^2}$	axial double velocity correlation
u_*	local wall friction velocity
u_{*sf}	local wall friction velocity in fully developed flow
u_i	fluctuating velocity component in x_i direction

V	mean radial velocity component
v	fluctuating radial velocity component
$\hat{v}$	root mean square value of v
$\overline{v^2}$	radial double velocity correlation
W	mean circumferential velocity
w	fluctuating circumferential velocity
$\hat{w}$	root mean square value of w
$\overline{w^2}$	circumferential double velocity correlation
x	axial cylindrical polar coordinate
x_i	cartesian coordinates x_1, x_2, x_3
y	distance measured from pipe wall along a radial line
y^+	defined by yu_*/ν
γ	effective viscosity of fluid
ε	rate of turbulent energy dissipation into heat per unit mass
ζ	relaxation factor
η	Kolmogorov microscale length
θ	azimuthal coordinate in cylindrical polar coordinate system
$\theta(\chi)$	phase-shift between u-v signals
κ	mixing length constant in effective viscosity model
λ	convergence criterion
ν	kinematic viscosity of the fluid
ν_T	eddy viscosity of the fluid

ξ	damping constant in effective viscosity model
ρ	density of the fluid
τ_s	wall shear stress
τ_{sf}	wall shear stress in fully developed flow
υ	Kolmogorov microscale velocity
$\phi_{u^2}(K)$	axial spectral density
ϕ	dependent variable in general elliptic equation
χ	non-dimensionalised wave-number
ψ	stream function
ω	mean vorticity
ω_{sf}	mean vorticity in fully developed flow

1. INTRODUCTION

Depending on the pipe Reynolds number, the condition of the entering flow and its approach, the flow in a cylindrical pipe can be laminar, partially laminar and turbulent, or turbulent along its entire length. In many cases the condition of the entering flow will be steady and uniform and will contain a small amount of residual turbulence due to its approach. If the pipe Reynolds number is high enough (say $Re > 2 \times 10^3$), it is possible by introducing an artificial disturbance at the pipe entrance, to cause the entering flow to form a turbulent boundary layer on the pipe wall, which grows in the downstream direction by molecular and turbulent mechanisms, until the boundary layer fills the whole of the pipe to form a mixing region. The flow then undergoes further adjustment until it becomes fully developed; i.e. independent of the downstream distance. The length of pipe required for the flow to become fully developed is called the inlet length and the region of fluid surrounded by the developing boundary layer, the entry core region. When such a flow has a constant fluid density, the flow which develops in the pipe is called a steady axi-symmetric incompressible turbulent flow. This type of flow, which is the subject

of investigation in this thesis, is shown schematically in Figure 1.

The importance of developing turbulent pipe flow has long been recognised in technology and is fundamental to the design of closed jet working sections for wind and water tunnels as well as for the design of tubular heat exchangers and hydraulic pipe systems. Nevertheless, the manner in which developing turbulent pipe flow adjusts from a boundary layer structure to a fully developed flow structure is not well understood. This stems from the fact that to date, all theoretical and experimental studies have been mainly confined to the flow in the pipe close to the inlet or far downstream, with very little consideration given to the mixing region which occurs when the boundary layer fills the whole of the pipe. Therefore, the purpose of the research to be reported in this thesis, will be to provide a better understanding of developing turbulent pipe flow and the manner in which it adjusts from a boundary layer type structure to a fully developed flow structure.

A statement of the problem can be formulated as follows:

"To produce a steady axi-symmetric incompressible developing turbulent pipe flow in the laboratory and investi-

gate its mean, time-averaged and spectral characteristics."

A brief outline of the current literature available on this problem is given in the next section.

1.1 Literature review

Published experimental data on the structure of developing turbulent pipe flow are very few, e.g. Holdhusen (1952), Barbin (1961), and Mizushina et al (1970). In Barbin's work, perhaps the most complete, some preliminary measurements of the mean velocity, turbulence intensities and Reynolds shear stress were reported for a single pipe Reynolds number ($Re = 3.88 \times 10^5$) in which fully developed flow was not attained. Difficulties encountered with the hot-wire equipment employed prevented Barbin from measuring the radial turbulence intensity field and component energy spectra. The work of Mizushina et al was confined to some turbulence measurements in the pipe inlet region and Holdhusen's, to measurement of head loss in the developing flow. Both Barbin's data and the present work dispute the findings of Mizushina et al that velocity profiles are similar in the developing flow. Current thoughts on the structure of fully developed pipe flow can be found in the papers of Laufer (1954) and Lawn (1971), who have made extensive measurements of the mean and turbulence field characteristics.

Although experimental data on developing turbulent pipe flow are rather meager, several semi-empirical analyses have been reported simulating mean flow characteristics in the initial part of the pipe inlet region. The first analysis was given by Latzko (1921), based on the Von Karman integral equation, using boundary layer assumptions and phenomenological concepts. Since that time many workers, e.g. Holdhusen (1952), Ross (1956), Fillipov (1958), and Bowlus and Brighton (1968) and Bradley and Cockrell (1970) have given improved analyses based on Latzko's original method. Reynolds (1968) in a morphology of prediction methods, considers how both differential and integral boundary layer techniques may be used to solve the problem of incompressible boundary layers using either a "turbulence equation of state" which relates the turbulence quantities to the properties of the mean field or a turbulent constitutive equation which relates the turbulence structure as reflected in the fluctuation correlations, to the turbulence energy and mean rate of strain. In a more recent review of boundary layer methods applied to internal fluid flow problems, Bradley and Cockrell (1970) discuss the limitations of the various methods and compare a solution of the Von Karman integral equation using an auxiliary relation with the data of Barbin (1961). Bradley and Cockrell admit their integral technique becomes less satisfactory for flow prediction especially after the boundary layer fills the whole of the pipe.

Other current prediction methods relying on turbulent constitutive equations and rational closure techniques have been reported in the literature by Daly and Harlow (1970), Donaldson (1971), Donaldson (1972), Fox and Lilly (1972) and others. Lumley and Khajeh-Nouri (1974) have given a critical review of these methods and pointed out a basic flaw. None of them present any method for generating the models used for third order terms. Lumley and Khajeh-Nouri proceed to present two related techniques which make it possible to generate in a straightforward and consistent manner, models of all third moments and of all orders of Reynolds numbers.

A basic conclusion which can be drawn from the literature reviewed is that the full potential of boundary layer and the more recent generation of prediction techniques cannot be realised until extensive and reliable information is obtained to serve as a basis for the formulation of auxiliary relationships and as a test case for theoretical solutions.

One approach not mentioned above which provides possibilities of simulating at least the mean flow parameters and shear stress fields in developing turbulent pipe flow, without new experimental data or auxiliary relationships can be found in the ideas of Gosman et al (1969). This approach will be pursued in Chapter 3.

1.2 Scope of the investigation

The scope of this investigation can be split into two parts. Firstly, the structure of steady axi-symmetric incompressible turbulent flow in the inlet length of a smooth pipe will be investigated through measurement of its mean, time-averaged and spectral characteristics for pipe Reynolds numbers of 1×10^5, 2×10^5, and 3×10^5. These measurements will be used to evaluate the terms appearing in the time-averaged energy equation to determine energy budgets for the flow field.

Secondly, a phenomenological flow model will be developed to simulate the mean flow, Reynolds shear stress and wall shear stress characteristics for comparison with the experimental measurements.

2. BASIC EQUATIONS

2.1 The time-averaged turbulence kinetic energy equation

Energy budgets for the developing turbulent pipe flow can be obtained from experimental evaluation of the terms in the time-averaged turbulence kinetic energy equation. The time-averaged energy equation written in mixed cylindrical polar and cartesian tensor coordinates has been derived by Huffman (1968) as

$$\underbrace{\frac{1}{2}\left(U\frac{\partial\overline{q^2}}{\partial x}+V\frac{\partial\overline{q^2}}{\partial r}\right)}_{\text{(I)}}+\underbrace{\left(\overline{uv}\left(\frac{\partial V}{\partial x}+\frac{\partial U}{\partial r}\right)+\overline{u^2}\,\frac{\partial U}{\partial x}+\overline{v^2}\,\frac{\partial V}{\partial r}\right)}_{\text{(II)}}$$

$$+\underbrace{\overline{\left(\frac{\partial}{\partial x}\left(\left\{\frac{uq^2}{2}+\frac{up}{\rho}\right\}\right)+\frac{1}{r}\frac{\partial}{\partial r}\left(r\left\{\frac{vq^2}{2}+\frac{vp}{\rho}\right\}\right)\right)}}_{\text{(III)}}$$

$$-\underbrace{\nu\left(\overline{\frac{\partial u_j}{\partial x_i}\frac{\partial u_i}{\partial x_j}}+\frac{1}{2}\nabla^2\overline{q^2}\right)}_{\text{(IV)}}+\underbrace{\nu\overline{\left(\frac{\partial u_i}{\partial x_j}+\frac{\partial u_j}{\partial x_i}\right)\frac{\partial u_j}{\partial x_i}}}_{\text{(V)}}=0 \qquad (2.1)$$

In the above equation an over bar represents time-averaging, U, V, W(=0) and u, v, w, denote the mean and fluctuating velocity components in the natural cylindrical polar coordinate system x, r and θ, p the fluctuating static

pressure, $\overline{q^2} = \overline{u^2} + \overline{v^2} + \overline{w^2}$ twice the turbulent kinetic energy per unit mass, u_i the fluctuating velocity component in the x_i direction and ρ and ν the fluid density and viscosity. The equation states that the sum of the convection of turbulence kinetic energy per unit mass (I), the production of turbulence energy (II), the convective diffusion by turbulence of the total turbulence energy (III), the work done per unit mass and of time by the viscous shear stresses of the turbulent motion (IV) and the rate of energy dissipation per unit mass by the turbulent motion (V) is zero. The sign convention adopted for (2.1) is such that if a term is positive, more energy is transported out of a volume element than is transported into a volume element, resulting in a net loss of energy in the volume element. Implicit in (2.1) are the conditions of flow axi-symmetry and symmetry of the Reynolds stress tensor. Given the quantities of U, $\overline{u^2}$, $\overline{v^2}$, $\overline{w^2}$ and $\overline{uv}$ from experiment and V computed from U via the continuity equation,

$$\frac{\partial U}{\partial x} + \frac{1}{r}\frac{\partial (rV)}{\partial r} = 0, \qquad (2.2)$$

terms (I), (II) and (IV) can be evaluated directly from the data with the exception of the first term in (IV), which can be neglected since according to Rotta (1962) viscous

diffusion is negligible except when the Reynolds number of the turbulence is very low, such as in the viscous sub-layer.

The dissipation (term (V)) can be evaluated using the dissipation rate ε calculated from measured u^2 energy spectra by the method proposed by Bradshaw (1967) as

$$\varepsilon = \left(\phi_{u^2}(K)^{-5/3}/0.53\right)^{3/2} \qquad (2.3)$$

In the above equation, which assumes the existence of local isotropy and an inertia subrange, $\phi_{u^2}(K)$ is the axial wave-number spectral density in the one-dimensional wave-number space K. Equation (2.1) can be employed to determine the diffusion (term III) as the closing entry in the energy balance.

2.2 Estimation of the local wall shear stress in developing turbulent pipe flow

A quantity of interest in developing turbulent pipe flow is the wall shear stress τ_s. In order to evaluate τ_s, two methods are considered.

In the first method, the wall shear stress is estimated from a cylindrical section of the fluid in the pipe of differential length dx. The difference between the momentum of the fluid entering and leaving the control volume must be balanced by the net pressure force acting across the cylinder and by the net force due to the wall shear stress acting around the cylinder circumference. Thus, the momentum balance can be written as

$$\frac{dM}{dx} = \frac{-dP}{dx} \pi R^2 - \tau_s 2\pi R \ , \tag{2.4}$$

where M the momentum of fluid entering the cylinder is given by

$$M = 2\pi\rho \int_o^R rU^2 dr \quad . \tag{2.5}$$

Combining (2.4) and (2.5), the local shear stress at the wall can be evaluated from

$$\tau_s = \frac{-R}{2} \frac{dP}{dx} - \frac{\rho}{2R} \frac{d}{dx} \left(\int_o^R U^2 (dr^2) \right) \tag{2.6}$$

by measurement of the wall static pressure gradient and axial velocities.

The second method considered for evaluation of the local wall shear stress is based on the law of the wall

$$U^+ = \frac{1}{k} \ln y^+ + C \quad , \tag{2.7}$$

where

$$U^+ = \frac{U}{u_*} \quad , \tag{2.8}$$

$$y^+ = \frac{y u_*}{\nu} \tag{2.9}$$

and u_* is defined by the relation

$$u_* = \sqrt{\tau_s/\rho} \quad . \tag{2.10}$$

The empirical constants k^* and C, according to Hirst and Coles (1968), should be given the values 0.41 and 5 respectively.

By substituting values of U and their corresponding values of y into (2.7), u_* can be evaluated by making the residuals

$$R_s = U^+ - \frac{1}{k} \ln y^+ - C \tag{2.11}$$

negligibly small. If the resulting values of u_* are plotted against y, the logarithmic region will correspond to constant values of the friction velocity for a particular velocity profile. Hirst and Coles suggest that only part of the axial velocity profile in the range $100<y^+<300$ be used to obtain u_* since close to the wall, high turbulence intensities and wall interference effects may cause pressure probe readings to be too high and farther from the wall, the wake-like outer structure of the developing turbulent boundary may be felt.

* It should be noted that the "constant" k is not really a constant. See Tennekes and Lumley (1972).

3. AN APPROXIMATE NUMERICAL SOLUTION FOR DEVELOPING TURBULENT PIPE FLOW

3.1 The mathematical model

The mathematical model is based on treating the turbulent flow as a laminar one with non-uniform viscosity, i.e. the fluid is considered to have an effective viscosity

$$\gamma = \rho(\nu + \nu_T) \tag{3.1}$$

consisting of a laminar and turbulent contribution.

The equations of motion in cylindrical polar co-ordinates using the idea of an effective viscosity have been given by Gosman et al (1969) as

$$\rho\left(U\frac{\partial U}{\partial x} + V\frac{\partial U}{\partial r}\right) = -\frac{\partial p}{\partial x} + \frac{\partial}{\partial x}\left(2\gamma\frac{\partial U}{\partial x}\right) + \frac{1}{r}\frac{\partial}{\partial r}\left(\gamma r\left(\frac{\partial U}{\partial r} + \frac{\partial V}{\partial x}\right)\right) \tag{3.2}$$

and

$$\rho\left(U\frac{\partial V}{\partial x} + V\frac{\partial V}{\partial r}\right) = -\frac{\partial p}{\partial r} + \frac{\partial}{\partial x}\left(\gamma\left(\frac{\partial U}{\partial r} + \frac{\partial V}{\partial x}\right)\right) + \frac{1}{r}\frac{\partial}{\partial r}\left(2\gamma r\frac{\partial V}{\partial r}\right) - \frac{2\gamma V}{r^2} \tag{3.3}$$

By differentiating (3.2) with respect to r, and (3.1) with respect to x, and subtracting one of the resulting equations from the other, the vorticity transport equation may be

written in the form

$$r^2\left(\frac{\partial}{\partial x}\left(\frac{\omega}{r}\frac{\partial\psi}{\partial r}\right)-\frac{\partial}{\partial r}\left(\frac{\omega}{r}\frac{\partial\psi}{\partial x}\right)\right)-\frac{\partial}{\partial x}\left(r^3\frac{\partial}{\partial x}\left(\frac{\gamma\omega}{r}\right)\right)-\frac{\partial}{\partial r}\left(r^3\frac{\partial}{\partial r}\left(\frac{\gamma\omega}{r}\right)\right)$$

$$-r^3S=0\quad, \tag{3.4}$$

where the term

$$S=\frac{-2}{r}\left(\frac{\partial^2\gamma}{\partial x^2}\frac{\partial U}{\partial r}-2\frac{\partial^2\gamma}{\partial r\partial x}\left(\frac{\partial U}{\partial x}-\frac{\partial V}{\partial r}\right)-\frac{\partial^2\gamma}{\partial r^2}\frac{\partial V}{\partial x}\right)\quad. \tag{3.5}$$

The mean vorticity ω is defined in terms of the stream function as

$$\omega=-\left(\frac{\partial}{\partial x}\left(\frac{1}{\rho r}\frac{\partial\psi}{\partial x}\right)+\frac{\partial}{\partial r}\left(\frac{1}{\rho r}\frac{\partial\psi}{\partial r}\right)\right)\quad, \tag{3.6}$$

and the stream function ψ which satisfies (2.2) defined through the relations

$$\frac{\partial\psi}{\partial r}=\rho Ur \tag{3.7}$$

and

$$\frac{\partial\psi}{\partial x}=-\rho Vr\quad. \tag{3.8}$$

Both the vorticity transport and stream function equations have an elliptic nature and can be expressed in a general form as

$$a\left[\frac{\partial}{\partial x}\left(\phi\,\frac{\partial\psi}{\partial r}\right)-\frac{\partial}{\partial r}\left(\phi\,\frac{\partial\psi}{\partial x}\right)\right]-\frac{\partial}{\partial x}\left[br\frac{\partial(c\phi)}{\partial r}\right]-\frac{\partial}{\partial r}\left[br\frac{\partial(c\phi)}{\partial r}\right]+rd=0\quad.\qquad(3.9)$$

for which ϕ and the coefficients a, b, c, and d for the vorticity and stream function equation are expressed in Table 1.

Simultaneous numerical solutions of the vorticity transport and stream function equations are now possible once suitable boundary and initial conditions and an effective viscosity model have been defined.

3.2 Boundary and initial conditions

Boundary conditions for the flow under consideration must be specified on closed surfaces representing the physical boundaries of the flow field. In formulating these conditions the following assumptions were made:

(i) the entering flow has uniform velocity U_b,

(ii) the boundary condition for the fully developed flow may be placed at a distance L = 100D on the basis that Comte-Bellot (1965) and others have concluded that fully developed turbulent pipe flow is generally achieved within 100 pipe diameters from the inlet,

(iii) close to the wall, gradients in the axial direction are much smaller than gradients in the radial direction,

(iv) U = V = 0 on the pipe wall and V = 0 along the pipe axis.

With these assumptions, the boundary conditions for ψ and ω can be derived as follows:

At the pipe entrance, ($x/D = 0$, $0 \leq y/R \leq 1$) Equation (3.7) can be integrated to give the stream function ψ_b at the pipe entrance as

$$\psi_b = \rho U_b r^2/2 + \psi_1 \quad , \tag{3.10}$$

where ψ_1 is a constant of integration. Since the flow entering the pipe is assumed uniform, the vorticity boundary condition at the pipe entrance is

$$\omega_b = 0 \quad . \tag{3.11}$$

At the pipe centre-line, ($0 \leq x/D \leq 100$, $y/R = 1$) the stream function from (3.10) becomes

$$\psi_c = \psi_1 \quad . \tag{3.12}$$

which simply expresses mass flux conservation. The corresponding vorticity boundary condition

$$\omega_c = 0 \quad . \tag{3.13}$$

At the downstream boundary, ($x/D \geq 100$, $0 \leq y/R \leq 1$) the gradients of ψ and ω in the axial direction are zero since the flow is fully developed, therefore the downstream

boundary conditions can be written as

$$\frac{\partial \psi}{\partial x} = 0 \tag{3.14}$$

and

$$\frac{\partial}{\partial x}\left(\frac{\omega}{r}\right) = 0 \quad . \tag{3.15}$$

At the pipe wall, $(0 \leq x/D \leq 100,\ y/R = 0)$, the boundary condition for the stream function from (3.10) becomes

$$\psi_s = \rho U_b R^2/2 + \psi_1 \quad . \tag{3.16}$$

In order to obtain the vorticity boundary condition ω_s, the vorticity ω is expanded through a first order Taylor expansion to give

$$\omega = \omega_s + y\left(\frac{\partial \omega}{\partial y}\right)_s \quad . \tag{3.17}$$

Very close to the wall the use of assumption (iii) reduces (3.6) to

$$\frac{\partial}{\partial y}\left[\frac{1}{\rho r}\frac{\partial \psi}{\partial y}\right] + \omega = 0 \quad , \tag{3.18}$$

providing a second relation between ψ and ω. Eliminating ω between (3.17) and (3.18), the resulting equation can be

integrated twice to yield

$$(\psi - \psi_s) + \rho\left(\frac{\partial\omega}{\partial y}\right)_s \left(\frac{Ry^3}{6} - \frac{y^4}{8}\right) + \rho\omega_s\left(\frac{Ry^2}{2} - \frac{y^3}{3}\right) = 0. \qquad (3.19)$$

Because the above equation can only be applied close to the wall, it can be reduced to give the vorticity boundary condition at the wall as

$$\omega_s = \left[\frac{2(\psi_s - \psi)}{\rho R y^2} - \left(\frac{\partial\omega}{\partial y}\right)_s \frac{y}{3} \right]_{y\to o} \qquad (3.20)$$

The initial conditions used to start the numerical analysis at interior points in the flow field were arbitrarily chosen as

$$\psi = \rho U_b R^2/2 \qquad (3.21)$$

and

$$\omega = 0 \quad . \qquad (3.22)$$

3.3 Effective viscosity model

Many proposals have been made in the literature for an effective viscosity model based on the law of the wall and the assumption of a uniform shear stress in the near wall region. These models have been designed in accord with experimental evidence from flows which do not have rapid streamwise variation of the wall shear stress. For a developing pipe flow in which the wall shear stress varies rapidly in the inlet region, a more general model is required. Of

several effective viscosity models considered for modification, the Van Driest (1956) model appeared to be the most amenable for use with the numerical solution method described in Section 3.4; primarily because it satisfied the following criteria.

(i) It was smooth and continuous in the near wall region.

(ii) It was devoid of velocity gradients inherent in the model structure which would considerably complicate the iterative finite difference technique and increase computing time and costs.

The form of the modified effective viscosity model used in the present analysis can be given as

$$\gamma = \frac{1}{2}\rho\nu\left(1 + \sqrt{1 + 4\kappa^2 y^{+2}(1 - \exp(-y^+/\xi))^2}\right) ,$$

for $0 \leq x/D \leq 100$ and $0 \leq y/R < 0.158$ (3.23)

and $$\gamma = (\gamma)_{y/R=0.158} ,$$

for $0 \leq x/D \leq 100$ and $0.158 \leq y/R \leq 1.$ (3.24)

The modification being a truncation of Van Driest's original model at $y/R = 0.158$* to give a constant effective viscosity in the range $0.158 \leq y/R \leq 1$, and allowing the model to be dependent on y^+ based on the local wall friction velocity u_*, to account for the rapid streamwise variation of the wall shear stress.

The justification for this latter modification can be found in Hirst and Coles (1968), where the local wall shear stress was evaluated using the law of the wall in flows with rapid streamwise variation in the wall shear stress. It is apparent that the success of the model depends on the choice of the damping constant ξ which controls the thickness of the viscous sub-layer and the mixing length constant κ which controls the slope of the turbulent portion of the velocity distribution. The constants ξ and κ were given the values of 0.41 and 26 respectively, to give velocity profiles, characteristic of fully developed flow in the range $5 \times 10^4 \leq Re \leq 5 \times 10^5$ when used with the truncated model with $0.158 \leq y/R \leq 1$.

Although the model might be expected to apply well in the fully turbulent flow regions, the assumption of a constant effective viscosity can hardly be expected to apply in the intermittent outer region of the turbulent boundary layer or in the entry core region. The intermittent nature of the outer region of the boundary layer would effect a decrease in the time-averaged viscosity, which would drop rapidly to a low effective viscosity characteristic of the entry core region. This objection, however, is not critical

* $y/R = 0.158$ was chosen to be compatible with a node in the finite difference grid described in Section 3.5.

to the final outcome of the numerical solutions since the mean velocity distribution outside of the wall region is rather insensitive to the assumed effective viscosity distribution. The behaviour of the effective viscosity in the intermittent and entry core regions will be discussed further in Section 5.3.

3.4 Numerical analysis

The basis for the numerical solution of the vorticity transport and stream function equations using the general elliptic form has been described by Gosman et al (1969) and will be summarised below.

Suppose the field of interest is covered by a non-linear grid network, the nodes in the grid corresponding to the intersection of the grid lines. Figure 2 shows a typical interior node P, and eight surrounding nodes; N, S, E, W, NE, NW, SE and SW. Integration of the general elliptic equation is performed over the broken line rectangle surrounding the point P, the sides of this rectangle denoted by the points n, s, e, w, ne, nw, se and sw lying midway between the neighbouring grid lines. In the integration, five assumptions are made.

(i) The average value of r^2 is the value at the centre of the rectangle $r_p{}^2$.

(ii) The value ϕ is uniform within each rectangle and assumes the prevailing value at the particular node

which the rectangle encloses.

(iii) The average value of ϕ at the point e takes on the ϕ value possessed by the fluid upstream of the e-face of the rectangle.

(iv) The value of the stream function ψ at the corner of the small rectangle is equal to the average of the values on the four neighbouring nodes.

(v) The term S is uniform over the area of integration and takes on the value at the point P.

With these assumptions, the integration of (3.9) can proceed to give the general finite difference formula for each variable at every interior node in the space as

$$\phi_P = \frac{\sum_{J=N,S,E,W} \left(\{A'_J + c_J(b_J+b_P)B'_J\} \phi_J \right) - d_P}{\sum_{J=N,S,E,W} \{A'_J + c_P(b_J+b_P)B'_J\}} \quad , \tag{3.25}$$

where the coefficients b, c, and d assume the appropriate values given in Table 1, and the A'_J's and B'_J's are given in Appendix A.

The boundary conditions are easily discretised since the ϕ values at the boundary nodes have the form

$$\phi = f \quad , \tag{3.26}$$

where f is a known constant or function. The algebraic sets of finite difference equations were solved simultan-

eously by a Gauss Seidel iterative method in which new values are used as soon as they are generated. Each cycle in the iterative procedure consists of two sub-cycles, one for each of the vorticity and stream function equations respectively. During the first sub-cycle, the field is scanned row by row and the independent variable ω, updated in the process. The second sub-cycle is then performed to obtain a new value of the dependent variable ψ, When the sub-cycles have been completed, a new iterative cycle is commenced; this procedure being repeated until converged solutions in ω and ψ are obtained. The iterative procedure was considered converged when the maximum fractional change in ϕ for the M^{th} iteration did not exceed a specified value λ, i.e.

$$\left| (\phi^{(M)} - \phi^{(M-1)})/\phi^{(M)} \right|_{MAX} \leq \lambda, \text{ for } \lambda \leq 0.001 \ . \quad (3.27)$$

Significant gains in convergence and stability were achieved by under-relaxing the vorticity and stream function equations with a relaxation factor ζ according to the relation

$$\phi = \zeta\phi^{(M)} + (1 - \zeta)\ \phi^{(M-1)}, \text{ for } \zeta = 0.75 \ . \quad (3.28)$$

3.5 Finite difference grid

The first step is to consider a finite number of points located in the flow field for which the finite

difference forms of (3.2) and (3.3) are assumed to be valid. The array of points is referred to as a "grid", and the points themselves are termed "nodes" of the grid. Where the gradients of the variables are steep, the nodes should be closer together, and where the gradients are shallow, the nodes may be further apart. Also, the grid is arranged so that the outermost nodal points correspond to the physical boundaries of the flow field.

A satisfactory finite difference grid format was achieved by having twenty nodal grid points at x/D = 0, 0.25, 0.5, 0.75, 1.5, 2, 3, 4, 5, 10, 20, 25, 30, 35, 40, 50, 60, 70, and 100, some of which were chosen to conform with measuring stations on the experimental rig described in Section 4.1. (Other axial grid formats were used when required.) In the radial direction, the pipe radius was divided into twenty equi-spaced distances. The first eighteen were retained and a further twelve grid nodes fitted in the two remaining spaces using a geometric progression of ratio 1:1.4, the nodes getting closer together as the wall is approached. This radial grid format was found to be sufficient for the pipe Reynolds number range considered and always enabled computation of points within the viscous sub-layer defined by $0 \leq y^+ \leq 7$ without the use of special wall functions.

3.6 Errors

In order to check for round-off errors, the numerical analyses were run first in single precision and then in double precision. Round-off errors were found to be negligible, differences occuring only in the third significant digit.

Truncation errors which arise through replacement of the actual equations with the finite difference equations, were checked by refining the grid. Again no appreciable differences were found in the solutions, differences occuring only in the fourth significant digit.

In the early stages of this work, numerical solutions with and without the term S were obtained for Re = 5×10^5. Comparison of the results showed that setting the S term to zero throughout the flow field produced errors of less than 1.2% and 0.2% in the vorticity and stream functions, respectively. (These percentage indications for the vorticity and stream function equations being representative of the regions which, according to boundary layer theory, would be identified with the boundary layer.) The reason for the slight effect of the term S on the numerical solution is due to the fact that streamwise derivatives of γ are involved and that velocity gradients such as $\partial V/\partial x$ and $\partial V/\partial r$ are small. Hence, to conserve computer time and improve convergence and stability, the term S was neglected in further calculations.

4. EXPERIMENTAL APPARATUS, MEASUREMENTS AND ERRORS

4.1 Experimental apparatus

The experiments for evaluation of the flow characteristics were conducted in an open circuit wind tunnel shown schematically in Figure 3. The basic air moving device was a centrifugal blower, with the fan set to give average velocities in the test section in the range 10 - 60 m/sec. Air was passed through screens and flow straighteners into a specially designed contraction cone of contraction ratio 89:1 to provide a flat velocity profile at the inlet of the working section. Since the contraction was found to give a laminar flow at the beginning of the test section, turbulent flow was promoted at the pipe inlet by a 9 cm. length of No. 16 sandpaper, inset around the circumference of the pipe at the beginning of the working section. The working section consisted of gun bored sections of steel pipe internally honed to a mirror finish. The sections were 10.16 cms. in diameter with a total length of 75 pipe diameters. Air from the test section was allowed to exit via a 4^{o} half angle diffuser, 71.96 cms. in length to reduce any upstream influence due to exit disturbances.

A Betz micromanometer was used in all pressure probe measurements and the DISA hot-wire equipment used

throughout consisted of two identical channels, one for each wire of a 55A39 x-probe. A single channel was used with a single-wire 55F14 boundary layer probe. The two channels consisted of DISA 55D01 constant temperature anemometers, 55D10 linearisers, 55D25 auxiliary units and 55A06 correlators. D.C. voltage components were measured using a 55D30 digital voltmeter and A.C. signals with a 55D35 root mean square (r.m.s.) voltmeter. Axial radial and circumferential frequency spectra were measured using DISA equipment in conjunction with a Hewlett Packard 3594A wave-analyser utilising addition, subtraction and multiplying circuits developed in the turbulence laboratory at the University of Manitoba. Cospectrum and phase-shift measurements were made using the DISA equipment in conjunction with two 55D26 conditioning and filtering circuits and a phase-shift circuit capable of giving a phase-shift of $90^{o} \pm 1^{o}$. All instantaneous hot-wire signals were monitored on a Tektronix type 502 dual beam oscilloscope.

4.2 Measurements

Mean velocity traverses were made with total probe and wall static taps and these were used to calibrate the hot-wire probes in the fully developed flow where conditions are reasonably well known. The total head probe consisted of a round tube of external and internal diameters of 1 mm. and 0.76 mm., with a flattened tip with internal dimensions of 2 mm. wide and 0.15 mm. deep. Static pressures from wall tappings at 20 locations on the test section,

(four tappings equispaced circumferentially at each location) were used to determine the friction velocity u_{*sf} in the fully developed flow.

Mean velocity data was obtained from radial traverses at several locations from the inlet to fully developed flow condition using a total head probe and wall static taps, single-wire boundary layer and x-probe. A single-wire boundary layer probe was used to measure the axial r.m.s. velocity $\tilde{u}$. A check on the $\tilde{u}$ measurements was made with the x-wire probe, which was also used to measure the radial and circumferential root mean square velocities $\tilde{v}$ and $\tilde{w}$ and the velocity correlation $\overline{uv}$. Measurement of the axial, radial and circumferential spectra was accomplished by manually scanning through the frequency spectrum with a fixed band-width of 10Hz using the wave-analyser, with addition, subtraction and multiplying circuits. Cospectrum and phase-shift measurements were made using the method of Bendat and Piersol (1966). The dual beam oscilloscope was used to give an approximate visualisation of the instantaneous spatial structure of the turbulence and to determine the outer limit beyond which no intermittent bursts of the boundary layer could be detected.

4.3 Errors

Error estimates reflecting the trend accuracy, rather than the absolute accuracy of the measurements were evaluated using the technique of Kline and McClintock (1953). The trend errors were considered to be comprised of two dis-

tinct types. Firstly, calibration errors of the instrumentation due to changes in experimental conditions (e.g. temperature and wire resistance changes), and secondly, the sum of errors induced by the design of the measuring instruments through which the signals are passed.

Employing the standard operational instrument accuracies quoted in the manufacturer's catalogues and the maximum observed variations in environmental and equipment conditions, the following trend percentage error estimates (rounded off upwards to the nearest percent) were evaluated for the measured data.

The maximum trend error in the mean axial velocity and bulk velocity (U_b) using pressure probes was estimated at ±1% and with hot-wire equipment, ±2%. Estimated maximum trend errors in the friction velocity, in the r.m.s. velocities and Reynolds shear stress were ±5%, ±3%, and ±5% respectively.

Apart from corrections to $\tilde{v}$, $\tilde{w}$ and $\overline{uv}$ for yaw sensitivity of the x-probe, no corrections were made to the measured data.

5. RESULTS AND DISCUSSION

Apart from a slight Reynolds number effect, no major differences in the flow characteristics could be discerned for the three Reynolds numbers investigated. Therefore, discussion will be limited mainly to results obtained at $Re = 3 \times 10^5$.

5.1 Preliminary results

In section 4.1 it was stated that the contraction cone was found to cause a laminar boundary layer to develop at the pipe inlet. Some experiments were performed utilizing the change in velocity distribution in the transition region to estimate the transition point of the laminar flow to turbulent flow. This was accomplished by moving a total head boundary layer probe parallel to the pipe wall at a distance corresponding to a maximum difference between the velocities in the laminar and turbulent flow regimes. On being moved across the transition point the total head probe showed an increase in the total pressure Q. The results of these experiments are shown in Figure 4, where Q_e is the total pressure of the entering flow at the pipe centre-line. The transition points (estimated as the mid-point between the maximum and minimum values of Q/Q_e) are at approximately $x/D = 3$, 4.5 and 8 for $Re = 3 \times 10^5$, 2×10^5 and 1×10^5. Figure 5 shows the transition points from Figure 4 and the results of Mizushina et al (1970) plotted as a function

of pipe Reynolds number. As the pipe Reynolds number increases, the transition point moves towards the pipe entrance.

In order to have a common origin for the developing turbulent boundary at all pipe Reynolds numbers considered, the turbulence promoting device described in Section 4.1 was used. From hot-wire measurements and boundary layer analysis the virtual origin of the turbulent boundary layer was estimated to be approximately 3 cms. upstream of the down-stream end of the turbulence promoter. For convenience, the down-stream end of the turbulence promoter was used as a datum for all subsequent axial measurements.

5.2 Oscillograph traces

By careful observation of the instantaneous hot-wire signals on the oscilloscope, it was possible to determine the distance from the wall beyond which no turbulent bursts could be detected. The approximate outer limit of the boundary layer intermittency shown in Figure 6, indicates the entry core region to shrink in cross-sectional area as the turbulent boundary layer develops, with interaction of the perimeter of the boundary layer surface beginning to occur at $x/D = 25$ on the pipe centre-line. By $x/D = 30$ the entry core region entirely disappears as the boundary layer fills the whole of the pipe. Oscillograph traces along the pipe centre-line between $x/D = 25$ and $x/D = 30$ showed the

flow to consist of slow alternations of turbulent and non-turbulent fluid, suggesting that small pockets of fluid from the core entry region become trapped in the turbulent boundary layer at x/D = 25 and eventually become entrained as the boundary layer fills the whole of the pipe.

5.3 Mean characteristics

Figure 7 shows the axial velocity profiles obtained from the total head probe and static pressure taps for Re = 3×10^5, normalised by the bulk velocity in the test U_b (= 42 m/sec.). At the pipe entrance (x/D = 0) the entering flow velocity profile is uniform. As the flow develops, the profiles show the fluid near the wall to be retarded while the fluid in the entry core region is accelerated. In the entry core region the velocity profiles remain uniform, but as the boundary layer fills the whole of the pipe at x/D = 30, the profiles become moderately peaked, the peak gradually subsiding to give a constant value at x/D = 70 as the velocity profiles become characteristic of a fully developed flow. This peaking first postulated by Bradley and Cockrell (1970) from Barbin's data and the velocity defect law, and labelled "velocity overshoot", is shown more clearly from consideration of the centre-line velocity given in the Figure 8, which shows the centre-line velocity in the mixing region to be higher than in the fully developed flow. Figure 9 shows comparisons of the axial

velocity profiles from experiment with those obtained from from the numerical analysis. Although agreement is seen to be quite reasonable over the whole of the developing flow, the numerical analysis does not exhibit the "overshoot" phenomenon and predicts the centre-line velocity to proceed asymptotically towards a fully developed flow. This point will be discussed further in Section 5.4. The ratio of the bulk to centre-line velocity at x/D = 70 which gives an indication of the degree of development of the flow, were 0.847, 0.84, and 0.826 for Reynolds numbers of 3×10^5, 2×10^5, and 1×10^5. These are in reasonable agreement with Lawn (1971) who reported values of 0.806 to 0.833 for $35{,}000 \leq Re \leq 250{,}000$ for an x/D = 59. Figure 10 compares the axial velocity data of Barbin (1961) with the results from the present numerical analysis and the integral method of Bradley and Cockrell (1970). It is seen that the numerical analysis gives better agreement with Barbin's data than the integral method, especially after x/D = 16.5, the approximate limit of validity for integral methods.

Mean vorticity profiles calculated from the axial and corresponding radial velocities using the relation

$$\omega = \frac{\partial V}{\partial x} - \frac{\partial U}{\partial r} \qquad (5.1)$$

are shown in Figure 11, compared with vorticity profiles

obtained from the numerical analysis. For convenience, the vorticity is normalised by the mean vorticity at the wall in fully developed flow ω_{sf} obtained from the numerical analysis. The y^+ values for the data were evaluated from the axial velocity profiles by the momentum method described in Section 2.2 and employing Equations (2.9) and (2.10). As a consequence of the effective viscosity model, the numerically obtained vorticity profiles display a high degree of similarity in the viscous sub-layer and buffer regions, defined by $0 \leq y^+ \leq 7$ and $7 < y^+ \leq 100$ and over a greater part of the logarithmic region defined approximately by $100 < y^+ \leq 1000$. In the remaining y^+ region, the vorticity gradually propagates outward from the pipe wall and increases in the downstream direction as the flow develops. The experimental data also shows this latter trend, but good agreement near the pipe centre-line is prevented due to difficulty in computing the vorticity from unsmoothed axial and radial velocity data.

Figure 12 shows a comparison of the local wall shear stress obtained from the momentum and law of the wall methods described in Section 2.2, the numerical analysis and the integral analysis of Bradley and Cockrell (1970). In the inlet range $2 \leq x/D \leq 7$, the numerical and integral analyses give very good agreement with the local wall shear stress obtained from the momentum method whereas values obtained from the law of the wall method appear lower. The law of the wall method cannot be expected to apply in the

initial inlet region because it is only strictly valid for flows with a constant or small streamwise variation in wall shear stress; e.g. fully developed pipe flow. After $x/D = 7$, the momentum and law of the wall methods and numerical analysis show the local wall shear stress to decrease asymptotically towards a fully developed value between $40 \leq x/D \leq 50$, whereas the integral method shows the local wall shear stress to become fully developed at $x/D \simeq 25$. Bradley and Cockrell (1970) admit that their integral technique becomes less satisfactory for flow prediction especially after the entry core region disappears.

5.4 Time-averaged characteristics

Figures 13, 14 and 15 show the r.m.s. velocities $\tilde{u}$, $\tilde{v}$ and $\tilde{w}$ normalised by the friction velocity u_{*sf} (=1.955 m/sec.) for the fully developed flow. At any point in the turbulent fluid, $\tilde{u}/u_{*sf} > \tilde{w}/u_{*sf} > \tilde{v}/u_{*sf}$, showing the turbulence to be anisotropic, the degree of anisotropy decreasing from the wall to the pipe centre-line.

Profiles of the turbulence shear stress $\rho\overline{uv}$ non-dimensionalised by ρu^2_{*sf} are shown in Figure 16. It can be seen that the shear stresses are slow to develop near the pipe centre-line at the start of the mixing region. It is this slow adjustment of the shear stresses which causes the mean axial velocity profiles to become moderately peaked near the pipe centre-line when the boundary layer fills the whole of the pipe, the peak gradually flattening to give a

shallow maximum as the shear stress adjusts towards a linear profile characteristic of fully developed flow. A similar phenomenon has been noted by Comte-Bellot (1965) and others in the region of interaction between boundary layers in steady two-dimensional duct flow.

The error estimates in Section 4 for $\tilde{u}$, $\tilde{v}$, $\tilde{w}$ and $\overline{uv}$ appear higher than reflected by the experimental data, since errors due to calibration drifts were always lower than the observed maximum variations in environment and instrument conditions. It should be noted that the accuracy of the trends of the data will be much better than the accuracy of the absolute values.

As mentioned in Section 3.3, the success of the numerical analysis hinges to a great extent on the effective viscosity model because it determines how the theoretical shear stress field develops. Since the laminar shear stress contribution to the total shear stress is small everywhere except near the pipe wall, the Reynolds shear stress data obtained from experiment can be compared with the total shear stress obtained from the analysis. This comparison given in Figure 17 for $Re = 3 \times 10^5$, shows quite reasonable agreement. It can be seen that the effect of the truncation of the effective viscosity model at $y/R = 0.158$ gives a slight discontinuity in the theoretical shear stress profiles as the fully developed case is approached, resulting in values approximately 5% higher at $y/R = 0.158$ than those obtained from experiment. At station $x/D = 30$, the theoretical

shear stress profile is developing more rapidly than the profile obtained from experiment. This would account, to some extent, for the numerical analysis not exhibiting the "overshoot" phenomenon found in the experimental velocity profiles, because once the mixing region is formed, the flow would be decelerated more quickly than in the real case.

A comparison of the normalised eddy viscosity obtained from the analysis and from experiment through the relation

$$\frac{\nu_T}{\nu} = \frac{\overline{uv}}{\nu} \Big/ \frac{\partial U}{\partial y} \qquad (5.2)$$

is shown in Figure 18 for Re = 3×10^5. The values computed from the experimental data agree reasonably well with the analysis over most of the turbulent flow region, but rapidly drop away from the assumed constant value in the intermittent outer region of the turbulent boundary layer and assumes very small values in the entry core region and in the mixing region. The disagreement of the assumed and actual eddy viscosity distribution in the turbulent boundary layer and entry core region is not critical to the overall quality of the numerical analysis in these regions because of the relative insensitivity of the mean velocity distribution to the assumed eddy viscosity distribution. The relative insensitivity of the mean velocity distribution was investigated by changing the assumed constant value to correspond more closely with the experimentally obtained values. Computed errors were less than 1%.

5.5 Spectral characteristics

Axial, radial, circumferential and cospectrum wave-number spectral densities were obtained from measured frequency spectral densities using Taylor's hypothesis. The resulting wave-number spectrum densities were non-dimensionalised and scaled using the Kolmogorov length and velocity microscales

$$\eta = (\nu^3/\varepsilon)^{\frac{1}{4}} \tag{5.3}$$

and

$$\upsilon = (\nu\varepsilon)^{\frac{1}{4}} \quad , \tag{5.4}$$

giving

$$E_{u_i u_j}(\chi) = \phi_{u_i u_j}(K)/\upsilon^2\eta \tag{5.5}$$

and

$$\chi = K\eta \quad . \tag{5.6}$$

The cross spectral densities $E_{uv}(\chi)$ and phase-shift measurements $\theta(\chi)$ were obtained from coincident $(C_{uv}(\chi))$ and quadrature $(Q_{uv}(\chi))$ spectral density functions using the relations

$$E_{uv}(\chi) = \sqrt{C_{uv}^2(\chi) + Q_{uv}^2(\chi)} \quad , \tag{5.7}$$

and

$$\theta(\chi) = \tan^{-1}\left[Q_{uv}(\chi)/C_{uv}(\chi)\right] \quad . \tag{5.8}$$

respectively.

The main spectral characteristics of developing turbulent pipe are shown by a few selected spectra in Figures 19, 20, 21, 22,and 23. It is apparent from Figure 19 that the axial energy spectra exhibit a $\chi^{-5/3}$ dependence for about one decade of χ indicating that an inertial sub-range can exist in the presence of shear, and justifying to some extent the use of Bradshaw's (1967) method for obtaining ε.

Corresponding radial and circumferential spectral profiles shown in Figures 20 and 21, are very similar throughout the developing flow, but their respective energy levels in the low wave-number range are much less than the corresponding axial spectral energy levels. The axial and radial spectra did not obey the isotropic relation

$$E_{v^2}(\chi) = \frac{1}{2}\left[E_{u^2}(\chi) - \chi \frac{\partial E_{u^2}(\chi)}{\partial \chi}\right] \qquad (5.9)$$

except in the high wave-number ranges, indicating the small scale turbulent structure to be isotropic in character and the large scale structure associated with the low wave-number ranges to be anisotropic. Close to the wall the figures show that the component spectra are almost invariant throughout the whole wave-number range as the flow develops.

Figure 19 shows a comparison of the axial spectra measured on the pipe centre-line in the mixing and fully developed regions, with the axial spectrum displaying the

maximum spectral energy in the low wave-number range measured in the developing turbulent boundary layer at x/D = 10. Where the boundary layer fills the whole of the pipe at the beginning of the mixing region, the spectral energy in the low wave-number range is higher than in the boundary layer and fully developed regions. The same trend is exhibited in the corresponding radial and circumferential spectra shown in Figures 20 and 21, but not in the cospectra in Figure 22. This suggests that the increase in spectral energy is due mainly to convective diffusion of turbulent energy in the low wave-number range. Comparison of the high wave-number range of the cospectral densities in Figure 22 with the high wave-number range of the other component spectra in Figures 19, 20 and 21 reveals that there is a small reduction in level relative to the component spectra. This points towards isotropy in the extreme wave-number ranges even though $\tilde{u} > \tilde{w} > \tilde{v}$. For the sake of completeness, measurements of the phase-shift $\theta(\chi)$ are shown in Figure 23. In cospectral densities measured near the wall the phase-shifts have the same trends being above 180^{o} for the large scale turbulence structure decreasing through the inertial subrange to be below 180^{o} for the small scale structure. The reverse is true for cospectral densities measured near the edge of the boundary layer and in the mixing and fully developed regions.

5.6 Energy balances

Figures 24, 25 and 26 show the terms in the energy equation non-dimensionalised by u_{*sf}^3/R at x/D = 10, 30 and 70, corresponding to the developing boundary layer region, mixing region and fully developed region. Perhaps the most striking feature of the energy balances is the manner in which each individual term adjusts as the flow develops from a boundary layer structure to a fully developed structure. It can be seen that the loss of turbulent energy by convection (I) diminishes in the downstream direction and disappears completely once the flow becomes uni-directional. This term is primarily responsible for the manner in which the normal stresses develop in the downstream direction and generally reflects the dependence of the turbulent flow on its upstream history.

Throughout the developing flow close to the wall, most of the gain in turbulence energy due to production (II) is dissipated there. In the outer part of the turbulent boundary layer and near the pipe centre-line in the mixing and fully developed regions, the production of turbulence energy is negligible. This gives substance to the idea that very little of the increase in spectral energy levels near the pipe centre-line in the mixing region can be due to production, but mainly due to the gain by convective diffusion of turbulence energy (III). It should be noted that in the turbulent flow the production term (II) is essentially $\overline{uv}\partial U/\partial r$, the remaining terms $\overline{uv}\partial V/\partial x$, $\overline{u^2}\partial U/\partial x$

and $\overline{v^2}\partial V/\partial r$ are of second order or more. The individual terms are shown in Tables 2, 3 and 4, along with the velocity gradients $\partial U/\partial x$, $\partial U/\partial r$, $\partial V/\partial x$, $\partial V/\partial r$ for $x/D = 10$, 30 and 70. In the entry core region there is some production of turbulence energy due to the residual turbulence in the accelerating flow through $\overline{u^2}\partial U/\partial x$, but this is of second order magnitude compared with the turbulence energy production in the turbulent part of the flow near the wall. In the fully developed flow near the pipe centre-line all of the increase in turbulence energy due to convective diffusion is dissipated. Inspection of term (IV) shows that the work done by the viscous shear stresses, on the turbulence motion, influences the flow only near the wall and disappears as the flow becomes developed.

Finally, the dissipation term (V) shows that dissipation of turbulence energy increases as the flow develops, and that most of the dissipation occurs close to the pipe wall.

6. CONCLUDING REMARKS

An experimental and theoretical study of the mean and turbulent flow properties of developing turbulent pipe flow at a Reynolds number of 3×10^5 has been described. Data presented have included measurements of oscillograph traces, mean velocity, turbulence intensities, Reynolds stress, and one-dimensional energy spectra. The data was used to evaluate the terms in the time-averaged energy equation with the convective diffusion of turbulence energy by kinetic and pressure effects determined as the closing entry in the energy balance.

The oscillograph traces indicated the entry core region to shrink in cross-sectional area as the turbulent boundary layer develops, with interaction of the perimeter of the boundary layer surface beginning to occur at $x/D = 25$, the entry core region entirely disappearing by $x/D = 30$ as the boundary layer fills the whole of the pipe.

An interesting feature of the flow is the peaking of the pipe centre-line velocity caused by the slow adjustment of the shear stresses in the mixing region. Consideration of the mean velocity, turbulence intensities and shear stress measurements show that developing turbulent pipe flow requires an entry length of some 60 - 70 pipe diameters before it assumes the characteristics of a fully developed flow. Within this entry length the turbulence is inhomogen-

eous and anisotropic, the degree of anisotropy decreasing from the pipe wall towards the pipe axis.

The spectrum measurements show that corresponding radial and circumferential spectra are very similar throughout the developing flow but that their energy levels are less than in the corresponding axial spectra which exhibit $\chi^{-5/3}$ dependence for about one decade of the non-dimensional wave-number χ. The spectra indicate the small scale turbulence structure to be isotropic even though $\hat{u} > \hat{w} > \hat{v}$, and the large scale structure associated with the low wave-number range to be anisotropic. Perhaps the most interesting conclusion to be drawn from the spectra is that they show that the dominant energy process occurring in the mixing region is due to convective diffusion of turbulence energy and that this energy is associated with the low wave-number range.

Confirmation that the convective diffusion of turbulence energy is the dominant energy process in the mixing region is also given by the energy balances derived from the measured data. Term II in the energy equation indicates that most of the gain in turbulence energy by production is due primarily to the $\overline{uv}\partial U/\partial r$ term, other production terms being at most of second order.

From the numerical analysis it has been shown that a reasonable simulation of the mean flow and Reynolds stress characteristics can be obtained. The failure of the analysis

to predict the velocity "overshoot" phenomenon can be attributed in some measure to the crudity of the effective viscosity model and the exclusion of the source term S.

7. RECOMMENDATIONS

The primary objective of this research was to obtain quantitative information on the manner in which developing turbulent pipe flow adjusts from a boundary layer structure to a fully developed flow structure. As pointed out in Section 1.2 the full potential of boundary layer prediction methods (or indeed any of the current generation of prediction methods) cannot be realised until they have been tested against extensive and reliable information. It is therefore strongly recommended that the present data serve as a basis for the formulation of auxiliary equations and as a test case for comparison of integral methods and also, serve as a basis for comparison of the turbulence models of Daly (1970), Donaldson (1971) and (1972), Fox and Lilly (1972) and others.

APPENDIX A

COEFFICIENTS IN EQUATION (3.25)

$$A'_J = A_J/V_P \tag{A.1}$$

and
$$B'_J = B_J/(b_J - b_P)V_P \quad , \tag{A.2}$$

where
$$V_P = \frac{r_P}{4}\,(x_E - x_W) \cdot (r_N - r_S) \quad , \tag{A.3}$$

$$A_E = \frac{a_P}{8}\,\{(\psi_{SE} + \psi_S - \psi_{NE} - \psi_N) + |\psi_{SE} + \psi_S - \psi_{NE} - \psi_N|\} \quad ,$$

$$A_W = \frac{a_P}{8}\,\{(\psi_{NW} + \psi_N - \psi_{SW} - \psi_S) + |\psi_{NW} + \psi_N - \psi_{SW} - \psi_S|\} \quad , \tag{A.4}$$

$$A_N = \frac{a_P}{8}\,\{(\psi_{NE} + \psi_E - \psi_{NW} - \psi_W) + |\psi_{NE} + \psi_E - \psi_{NW} - \psi_W|\} \quad ,$$

$$A_S = \frac{a_P}{8}\,\{(\psi_{SW} + \psi_W - \psi_{SE} - \psi_E) + |\psi_{SW} + \psi_W - \psi_{SE} - \psi_E|\}$$

and
$$B_E = \frac{b_E + b_P}{8} \cdot \frac{r_N - r_S}{x_E - x_P} \cdot (r_E + r_P) \quad ,$$

$$B_W = \frac{b_W + b_P}{8} \cdot \frac{r_N - r_S}{x_P - x_W} \cdot (r_W + r_P) \quad , \tag{A.5}$$

$$B_N = \frac{b_N + b_P}{8} \cdot \frac{x_E - x_W}{r_N - r_P} \cdot (r_N + r_P) \quad ,$$

$$B_S = \frac{b_S + b_P}{8} \cdot \frac{x_E - x_W}{r_P - r_S} \cdot (r_S + r_P) \quad .$$

REFERENCES

BARBIN, A.R. 1961 Development of turbulence in the inlet of a smooth pipe. Ph.d Thesis, Purdue University.

BENDAT, J.S. AND PIERSOL, E.G. 1966 Measurement and analysis of random signals. John Wiley, p. 275.

BRADLEY, C.I. AND COCKRELL, D.J. 1970 Boundary layer methods applied to internal fluid problems. Proceedings of the Heat Transfer and Fluid Mechanics Institute. Stanford University Press.

BRADSHAW, P. 1967 Conditions for the existence of an inertial subrange in turbulent flow. N.P.L. Aero Rept. 1220.

BOWLUS, D.A. AND BRIGHTON, J.A. 1968 Incompressible flow in the inlet region of a smooth pipe. Journ. Basic Eng. Trans A.S.M.E. Series D, 90.

COMTE-BELLOT, G. 1965 Ecoulement turbulent entre deux parois paralleles. Pub. Sci. et Tech. du ministère de l'air, No. 419.

DALY, B.J. AND HARLOW, F.M. 1970 Transport equations in turbulence. Phys. Fluids, 13.

DONALDSON, C.D. 1971 Calculation of turbulent shear flows for atmospheric and vortex motions. AIAA.J., 10

DONALDSON, C.D. 1972 Construction of a dynamic model of the production of atmospheric turbulence and dispersal of atmospheric pollutants. Am. Meteor. Soc.

FILLIPOV, G.V. 1958 On turbulent flow in the entrance length of a straight tube of circular cross-section. Soviet Physics - Technical Physics, 32, 8.

FOX, D.G. AND LILLY, D.K. 1972 Numerical simulation of turbulent flows. Rev. Geo. and Space Physics, 10.

GOSMAN, A.D., PUN, W.M., RUNCHAL, A.D., SPALDING, D.B. AND WOLFSHSTEIN, M. 1969 Heat and mass transfer in recirculating flows. Academic Press.

HIRST, D.E. AND COLES, E.A. (eds.) 1968) Computation of turbulent boundary layers. Proceedings (1968) AFOSR-IFP-Stanford Conference, vol. 2, Stanford University Press.

HOLDHUSEN, J.S. 1952 The turbulent boundary layer in the inlet region of a smooth pipe. Ph.d Thesis, University of Minnesota.

HUFFMAN, G.D. 1968 A theoretical analysis of turbulent shear flows. Ph.d Thesis, Ohio State University.

KHAJEH-NOURI, B. AND LUMLEY, J.L. 1974 Computational modelling of turbulent flows. (Submitted to Phys. Fluids.)

KLINE, S.J. AND McCLINTOCK, F.A. 1953 Describing uncertainties in single-sample experiments, Mech. Eng. 3.

LATZKO, H. 1921 Der warmeiibergang an unin turbulenten flussigkeits oder gasstrom. Zeits. fur ang. Math. und Mech., 1, 4.

LAUFER, J. 1954 The structure of turbulence in fully developed pipe flow. NACA Rept. 1174.

LAWN, C.J. 1971 Rate of dissipation in turbulent pipe flow. J. Fluid Mech., 48, 477.

MIZUSHINA, T., RYUSO, L., HIROMASA, U., SHIGEKA, T., AND HIDEO, M. 1970 Some turbulence measurements in the inlet of a circular pipe. J. Chem. Eng. Japan, 3, 1.

ROSS, D. 1956 Turbulent flow in the entrance region of a pipe. Trans. A.S.M.E., 78.

ROTTA, J.C. 1962 Turbulent boundary layers in incompressible flow. Pergamon Press.

TENNEKES, H. AND LUMLEY, J.L. 1972 A first course in turbulence. The M.I.T. Press, Cambridge.

VAN DRIEST, E.R. 1956 On turbulent flow near a wall. J. Aero. Sci., 23.

FUNCTION / EQUATION	ϕ	a	b	c	d
STREAM FUNCTION	ψ	0	$\frac{1}{\rho r^2}$	1	$-\frac{\omega}{r}$
VORTICITY TRANSPORT	$\frac{\omega}{r}$	r^2	r^2	γ	$r^2 S$

TABLE 1. Functions ϕ, a, b, c and d.

r/R	$\overline{u^2}\partial U/\partial x$	$\overline{v^2}\partial V/\partial r$	$\overline{uv}\partial U/\partial r$	$\overline{uv}\partial V/\partial x$
0.000E 00	0.000E 00	0.000E 00	0.000E 00	0.000E 00
0.500E-01	0.279E-02	-0.134E-02	0.000E 00	0.000E 00
0.100E 00	0.279E-02	-0.890E-03	0.000E 00	0.000E 00
0.150E 00	0.272E-02	-0.890E-03	0.000E 00	0.000E 00
0.200E 00	0.272E-02	-0.890E-03	0.000E 00	0.000E 00
0.250E 00	0.272E-02	-0.890E-03	0.000E 00	0.000E 00
0.300E 00	0.369E-02	-0.856E-03	0.000E 00	0.000E 00
0.350E 00	0.542E-02	-0.109E-02	0.000E 00	0.591E-06
0.400E 00	0.678E-02	-0.887E-03	-0.204E-01	0.300E-05
0.450E 00	0.573E-02	-0.307E-04	-0.107E 00	0.105E-04
0.500E 00	0.457E-02	0.167E-02	-0.370E 00	0.263E-04
0.550E 00	-0.778E-02	0.371E-02	-0.102E 01	0.520E-04
0.600E 00	-0.623E-03	0.477E-02	-0.186E 01	0.733E-04
0.650E 00	-0.140E-01	0.697E-02	-0.297E 01	0.828E-04
0.700E 00	-0.262E-01	0.110E-01	-0.415E 01	0.486E-04
0.750E 00	-0.551E-01	0.154E-01	-0.686E 01	-0.560E-04
0.800E 00	-0.652E-01	0.154E-01	-0.100E 02	-0.274E-03
0.850E 00	-0.262E-01	0.862E-02	-0.129E 02	-0.561E-03
0.900E 00	0.104E-01	-0.139E-02	-0.174E 02	-0.716E-03
0.950E 00	0.339E-01	-0.456E-02	-0.294E 02	-0.740E-03
0.970E 00	-0.595E-02	0.468E-02	-0.257E 03	-0.740E-03
0.100E 01	0.000E 00	0.000E 00	0.000E 00	0.000E 00

TABLE 2. Turbulence energy production and velocity gradient terms x/D = 10.

(Note: The production terms have been non-dimensionalised by u^3_{*sf}/R)

r/R	∂u/∂x	∂U/∂r	∂V/∂x	∂V/∂r
0.000E 00	0.257E 01	0.149E-01	0.000E 00	-0.321E 01
0.500E-01	0.257E 01	0.000E 00	-0.764E-03	-0.193E 01
0.100E 00	0.257E 01	-0.745E-02	-0.903E-03	-0.129E 01
0.150E 00	0.257E 01	-0.745E-02	-0.879E-03	-0.129E 01
0.200E 00	0.257E 01	0.000E 00	-0.693-03	-0.129E 01
0.250E 00	0.257E 01	0.000E 00	-0.100E-03	-0.129E 01
0.300E 00	0.257E 01	0.000E 00	0.979E-03	-0.124E 01
0.350E 00	0.238E 01	0.000E 00	0.288E-02	-0.105E 01
0.400E 00	0.198E 01	-0.401E 02	0.589E-02	-0.609E 00
0.450E 00	0.110E 01	-0.100E 03	0.984E-02	-0.155E-01
0.500E 00	0.617E 00	-0.200E 03	0.142E-01	0.678E 00
0.550E 00	-0.746E 00	-0.341E 03	0.173E-01	0.116E 01
0.600E 00	-0.489E-01	-0.441E 03	0.174E-01	0.117E 01
0.650E 00	-0.819E 00	-0.481E 03	0.134E-01	0.134E 01
0.700E 00	-0.120E 01	-0.501E 03	0.587E-02	0.180E 01
0.750E 00	-0.206E 01	-0.642E 03	-0.524E-02	0.217E 01
0.800E 00	-0.203E 01	-0.742E 03	-0.203E-01	0.189E 01
0.850E 00	-0.697E 00	-0.762E 03	-0.333E-01	0.855E 00
0.900E 00	0.255E 00	-0.922E 03	-0.378E-01	-0.125E 00
0.950E 00	0.733E 00	-0.130E 04	-0.327E-01	-0.341E 00
0.970E 00	-0.110E 00	-0.956E 04	-0.275E-01	0.293E 00
0.100E 01	0.000E 00	-0.340E 05	0.000E 00	0.202E 01

TABLE 2. (continued)

r/R	$\overline{u^2}\partial U/\partial x$	$\overline{v^2}\partial V/\partial r$	$\overline{uv}\partial U/\partial r$	$\overline{uv}\partial V/\partial x$
0.000E 00	0.000E 00	0.000E 00	0.000E 00	0.000E 00
0.500E-01	-0.201E-02	0.121E-02	-0.689E-01	0.267E-05
0.100E 00	-0.496E-02	0.175E-02	-0.157E 00	0.837E-05
0.150E 00	-0.571E-02	0.272E-02	-0.460E 00	0.171E-04
0.200E 00	-0.137E-01	0.469E-02	-0.703E 00	0.215E-04
0.250E 00	-0.218E-01	0.699E-02	-0.950E 00	0.305E-04
0.300E 00	-0.285E-01	0.680E-02	-0.138E 01	0.338E-04
0.350E 00	-0.182E-01	0.467E-02	-0.187E 01	0.323E-04
0.400E 00	-0.260E-01	0.394E-02	-0.254E 01	0.252E-04
0.450E 00	-0.248E-01	0.394E-02	-0.291E 01	0.790E-05
0.500E 00	-0.289E-01	0.371E-02	-0.315E 01	-0.125E-04
0.550E 00	-0.293E-01	0.346E-02	-0.382E 01	-0.354E-04
0.600E 00	-0.299E-01	0.284E-02	-0.491E 01	-0.555E-04
0.650E 00	-0.293E-01	0.245E-02	-0.612E 01	-0.696E-04
0.700E 00	-0.319E-01	0.148E-02	-0.689E 01	-0.730E-04
0.750E 00	-0.191E-01	0.119E-03	-0.931E 01	-0.603E-04
0.800E 00	-0.265E-01	-0.220E-03	-0.120E 02	-0.461E-04
0.850E 00	-0.224E-01	-0.320E-02	-0.145E 02	-0.363E-04
0.900E 00	0.226E-01	-0.135E-01	-0.345E 02	-0.191E-04
0.950E 00	0.858E-01	-0.316E-01	-0.219E 02	-0.166E-03
0.970E 00	0.140E 00	-0.878E-01	-0.203E 03	-0.250E-03
0.100E 01	0.000E 00	0.000E 00	0.000E 00	0.000E 00

TABLE 3. Turbulence energy production and velocity gradient terms x/D = 30.

(Note: The production terms have been non-dimensionalised by u^3_{*sf}/R)

r/R	∂U/∂x	∂U/∂r	∂V/∂x	∂V/∂r
0.000E 00	-0.149E 00	-0.217E 03	0.000E 00	0.149E 00
0.500E-01	-0.248E 00	-0.986E 02	0.383E-02	0.248E 00
0.100E 00	-0.546E 00	-0.986E 02	0.525E-02	0.339E 00
0.150E 00	-0.546E 00	-0.178E 03	0.658E-02	0.503E 00
0.200E 00	-0.114E 01	-0.197E 03	0.703E-02	0.833E 00
0.250E 00	-0.154E 01	-0.217E 03	0.697E-02	0.113E 01
0.300E 00	-0.174E 01	-0.256E 03	0.629E-02	0.101E 01
0.350E 00	-0.945E 00	-0.296E 03	0.511E-02	0.640E 00
0.400E 00	-0.114E 01	-0.335E 03	0.332E-02	0.480E 00
0.450E 00	-0.947E 00	-0.335E 03	0.910E-03	0.441E 00
0.500E 00	-0.948E 00	-0.316E 03	-0.125E-02	0.378E 00
0.550E 00	-0.849E 00	-0.335E 03	-0.311E-02	0.319E 00
0.600E 00	-0.751E 00	-0.375E 03	-0.423E-02	0.237E 00
0.650E 00	-0.653E 00	-0.414E 03	-0.471E-02	0.184E 00
0.700E 00	-0.654E 00	-0.434E 03	-0.460E-02	0.107E 00
0.750E 00	-0.357E 00	-0.533E 03	-0.345E-02	0.789E-02
0.800E 00	-0.458E 00	-0.631E 03	-0.243E-02	-0.138E-01
0.850E 00	-0.360E 00	-0.710E 03	-0.179E-02	-0.186E 00
0.900E 00	0.333E 00	-0.158E 04	-0.873E-03	-0.748E 00
0.950E 00	0.122E 01	-0.958E 03	-0.725E-02	-0.164E 01
0.970E 00	0.192E 01	-0.839E 04	-0.103E-01	-0.425E 01
0.100E 01	0.000E 00	-0.324E 05	0.000E 00	-0.114E 02

TABLE 3. (continued)

r/R	$\overline{u^2}\partial U/\partial x$	$\overline{v^2}\partial V/\partial r$	$\overline{uv}\partial U/\partial r$	$\overline{uv}\partial V/\partial x$
0.000E 00	0.000E 00	0.000E 00	0.000E 00	0.000E 00
0.500E-01	0.000E 00	0.000E 00	-0.600E-01	-0.362E-05
0.100E 00	0.000E 00	0.000E 00	-0.192E 00	-0.105E-04
0.150E 00	0.000E 00	0.000E 00	-0.379E 00	-0.146E-04
0.200E 00	0.000E 00	0.000E 00	-0.448E 00	-0.190E-04
0.250E 00	0.000E 00	0.000E 00	-0.648E 00	-0.200E-04
0.300E 00	0.000E 00	0.000E 00	-0.105E 01	-0.195E-04
0.350E 00	0.000E 00	0.000E 00	-0.149E 01	-0.165E-04
0.400E 00	0.000E 00	0.000E 00	-0.238E 01	-0.155E-04
0.450E 00	0.000E 00	0.000E 00	-0.227E 01	-0.198E-04
0.500E 00	0.000E 00	0.000E 00	-0.359E 01	-0.191E-04
0.550E 00	0.000E 00	0.000E 00	-0.533E 01	-0.142E-04
0.600E 00	0.000E 00	0.000E 00	-0.513E 01	-0.228E-04
0.650E 00	0.000E 00	0.000E 00	-0.617E 01	-0.448E-04
0.700E 00	0.000E 00	0.000E 00	-0.674E 01	-0.696E-04
0.750E 00	0.000E 00	0.000E 00	-0.833E 01	-0.920E-04
0.800E 00	0.000E 00	0.000E 00	-0.107E 02	-0.103E-03
0.850E 00	0.000E 00	0.000E 00	-0.146E 02	-0.984E-04
0.900E 00	0.000E 00	0.000E 00	-0.188E 02	-0.100E-03
0.950E 00	0.000E 00	0.000E 00	-0.539E 02	-0.106E-03
0.970E 00	0.000E 00	0.000E 00	-0.228E 03	-0.936E-04
0.100E 01	0.000E 00	0.000E 00	0.000E 00	0.000E 00

TABLE 4. Turbulence energy production and velocity gradient terms x/D = 70.

(Note: The production terms have been non-dimensionalised by u^3_{*sf}/R)

r/R	∂U/∂x	∂U/∂r	∂V/∂x	∂V/∂r
0.000E 00	0.000E 00	-0.235E 02	0.000E 00	0.000E 00
0.500E-01	0.000E 00	-0.415E 02	-0.251E-02	0.000E 00
0.100E 00	0.000E 00	-0.686E 02	-0.376E-02	0.000E 00
0.105E 00	0.000E 00	-0.921E 02	-0.354E-02	0.000E 00
0.200E 00	0.000E 00	-0.831E 02	-0.354E-02	0.000E 00
0.250E 00	0.000E 00	-0.101E 03	-0.312E-02	0.000E 00
0.300E 00	0.000E 00	-0.134E 03	-0.248E-02	0.000E 00
0.350E 00	0.000E 00	-0.161E 03	-0.178E-02	0.000E 00
0.400E 00	0.000E 00	-0.228E 03	-0.149E-02	0.000E 00
0.450E 00	0.000E 00	-0.193E 03	-0.168E-02	0.000E 00
0.500E 00	0.000E 00	-0.276E 03	-0.147E-02	0.000E 00
0.550E 00	0.000E 00	-0.378E 03	-0.100E-02	0.000E 00
0.600E 00	0.000E 00	-0.336E 03	-0.150E-02	0.000E 00
0.650E 00	0.000E 00	-0.369E 03	-0.267E-02	0.000E 00
0.700E 00	0.000E 00	-0.370E 03	-0.382E-02	0.000E 00
0.750E 00	0.000E 00	-0.421E 03	-0.465E-02	0.000E 00
0.800E 00	0.000E 00	-0.504E 03	-0.489E-02	0.000E 00
0.850E 00	0.000E 00	-0.663E 03	-0.447E-02	0.000E 00
0.900E 00	0.000E 00	-0.849E 03	-0.453E-02	0.000E 00
0.950E 00	0.000E 00	-0.233E 04	-0.457E-02	0.000E 00
0.970E 00	0.000E 00	-0.104E 05	-0.425E-02	0.000E 00
0.100E 01	0.000E 00	-0.328E 05	0.000E 00	0.000E 00

TABLE 4. (continued)

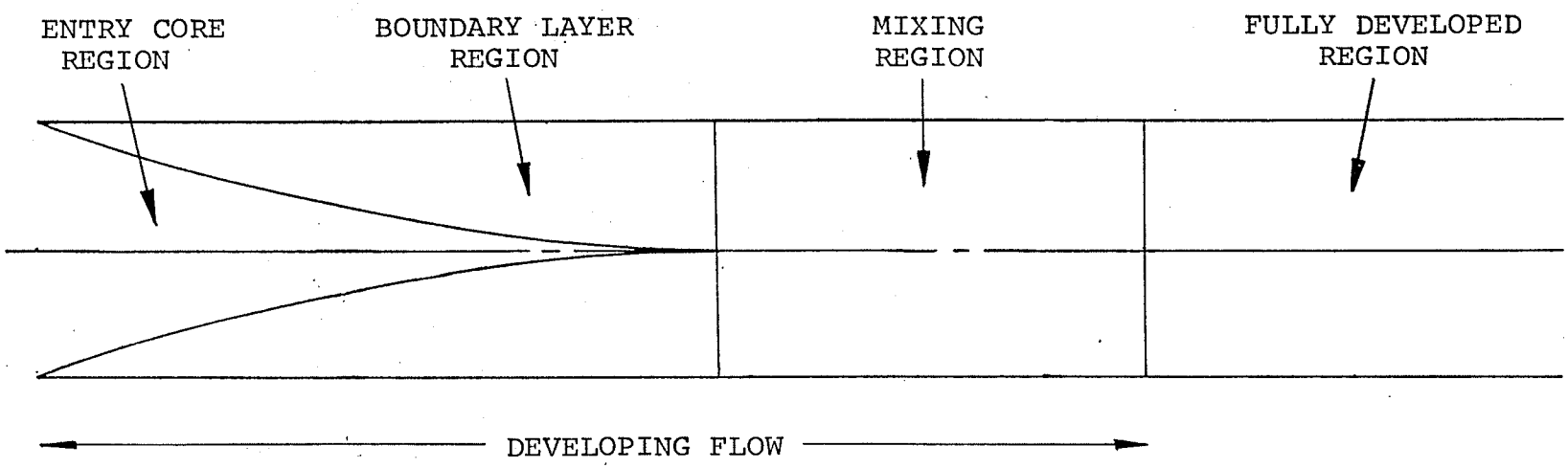

FIGURE 1. Idealised model of developing turbulent pipe flow.

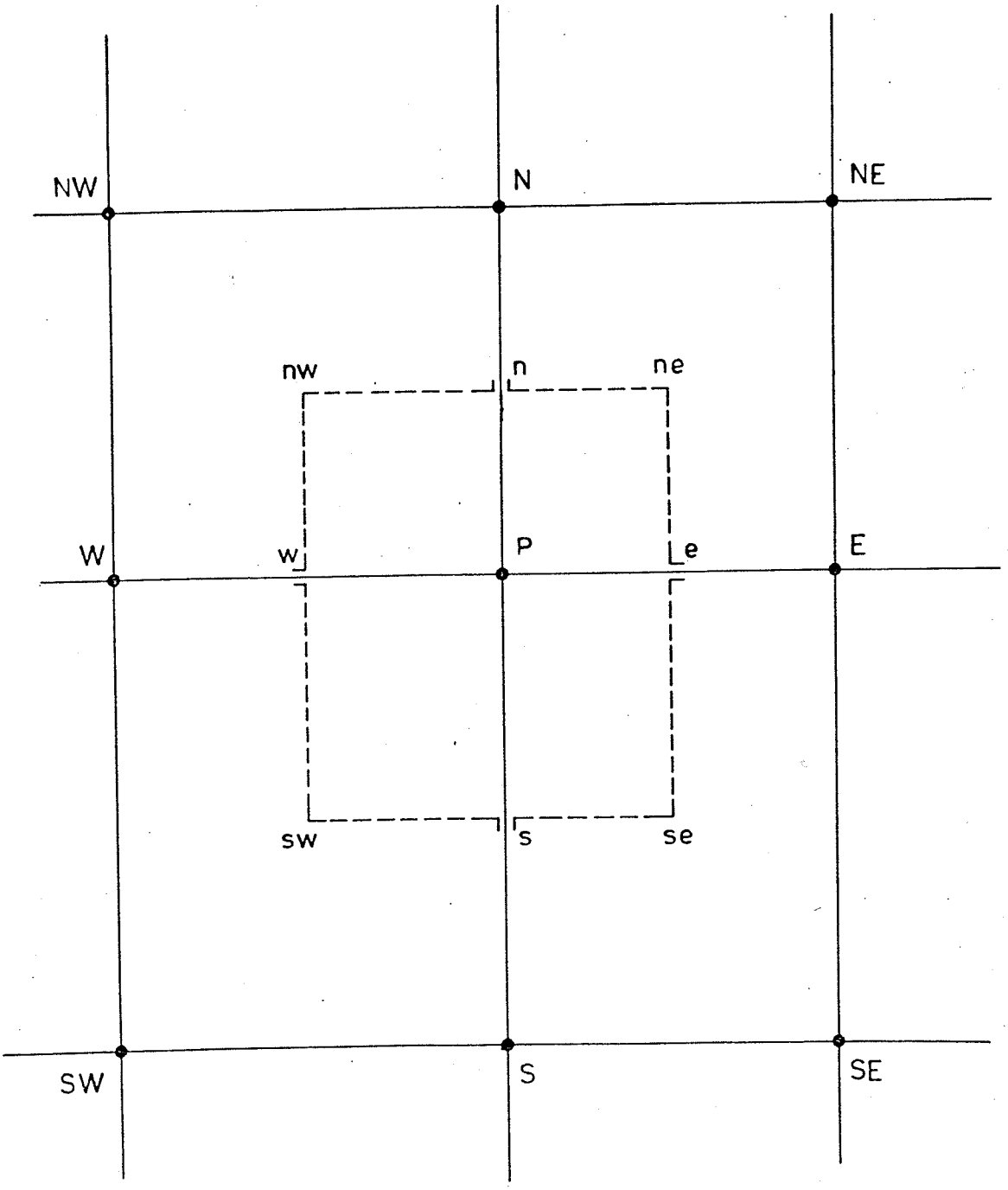

FIGURE 2. Interior node P in the finite difference grid.

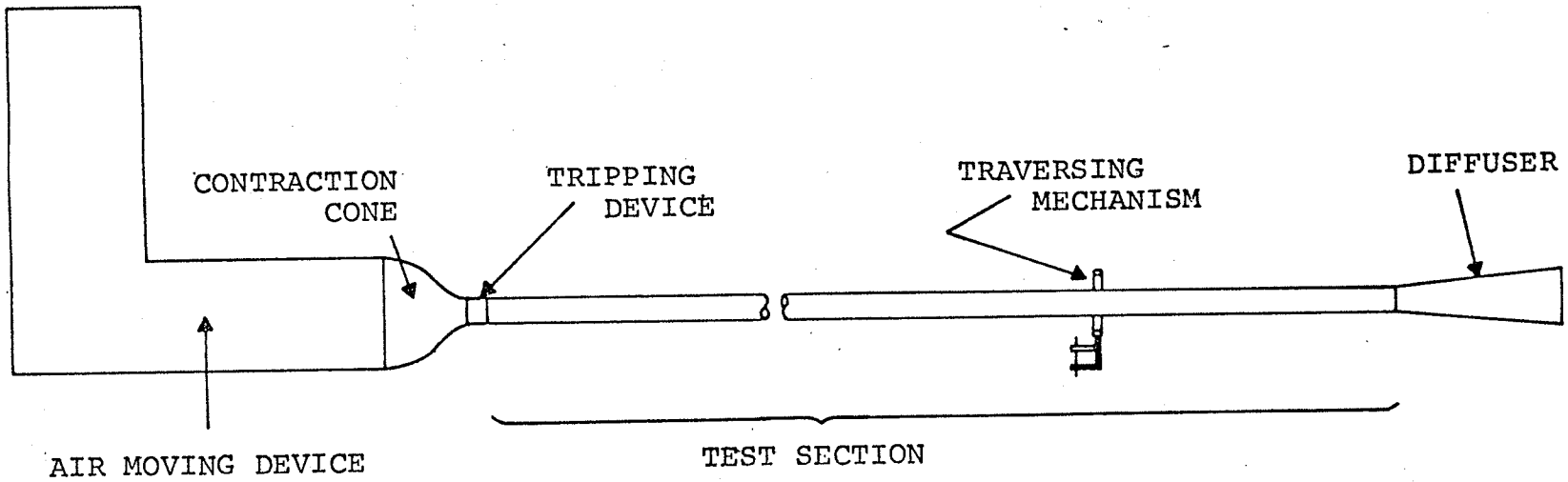

FIGURE 3. Schematic diagram of wind tunnel apparatus.

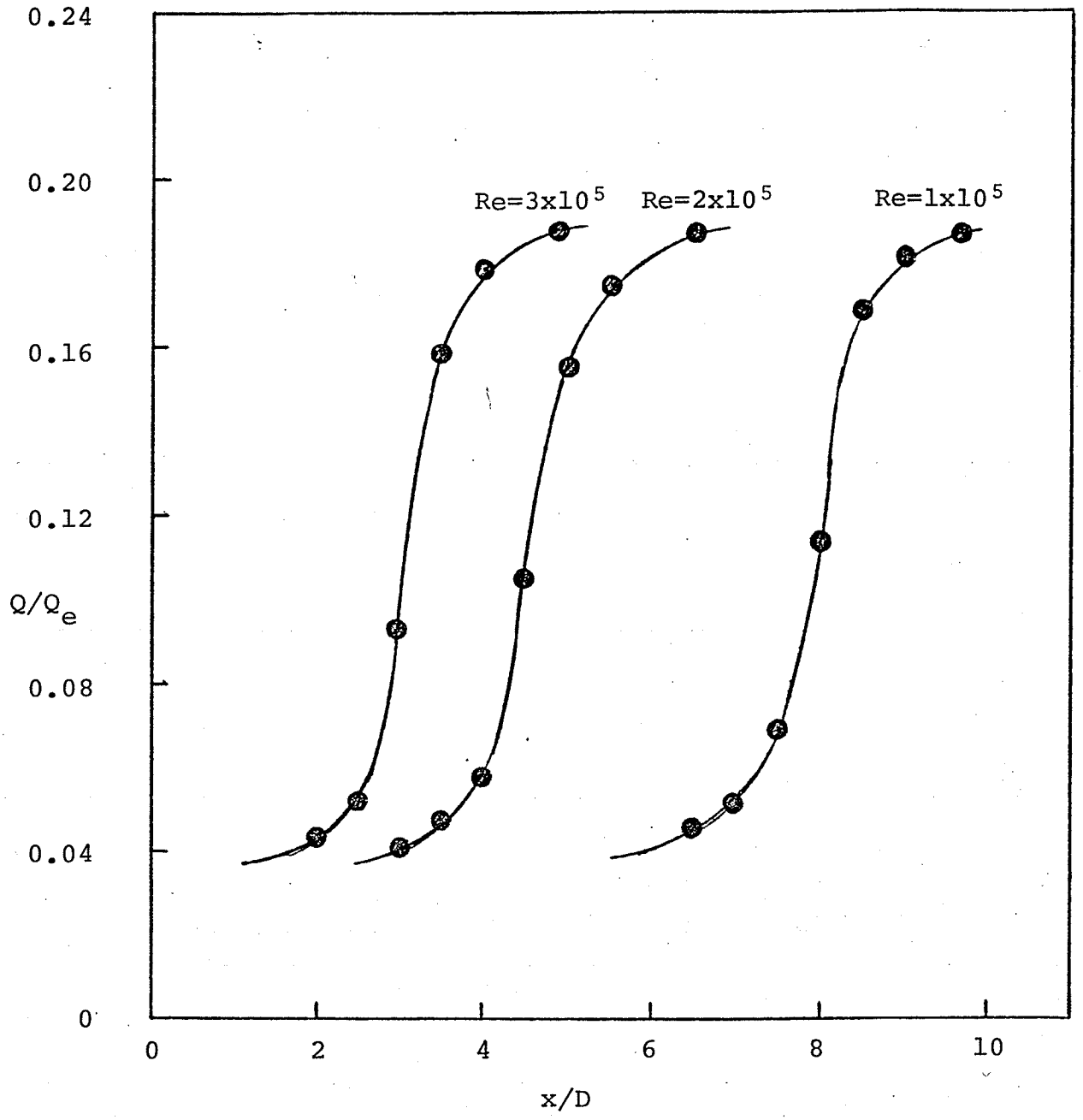

FIGURE 4. Total pressure plot for estimation of transition point.

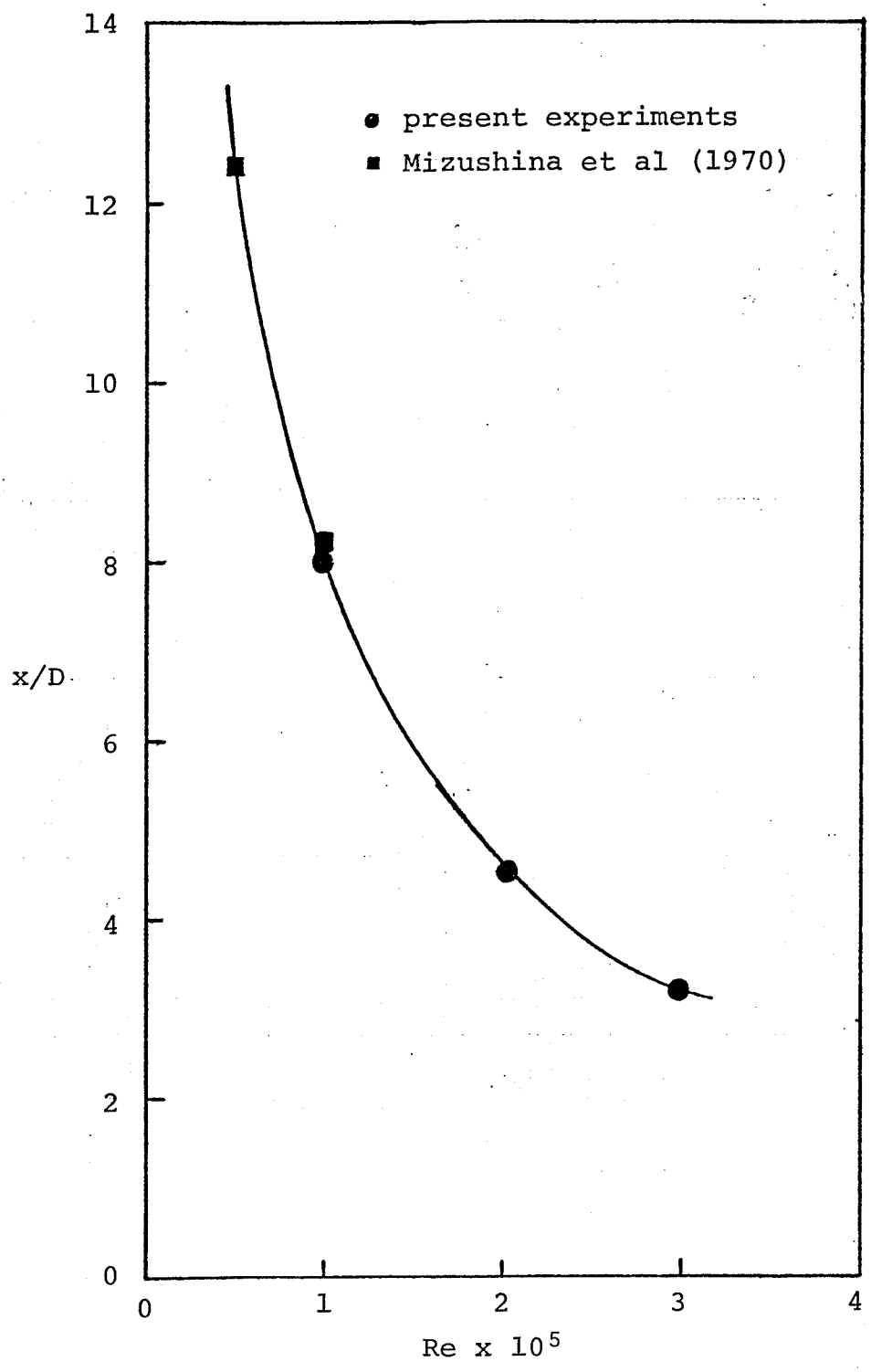

FIGURE 5. Transition point versus pipe Reynolds number.

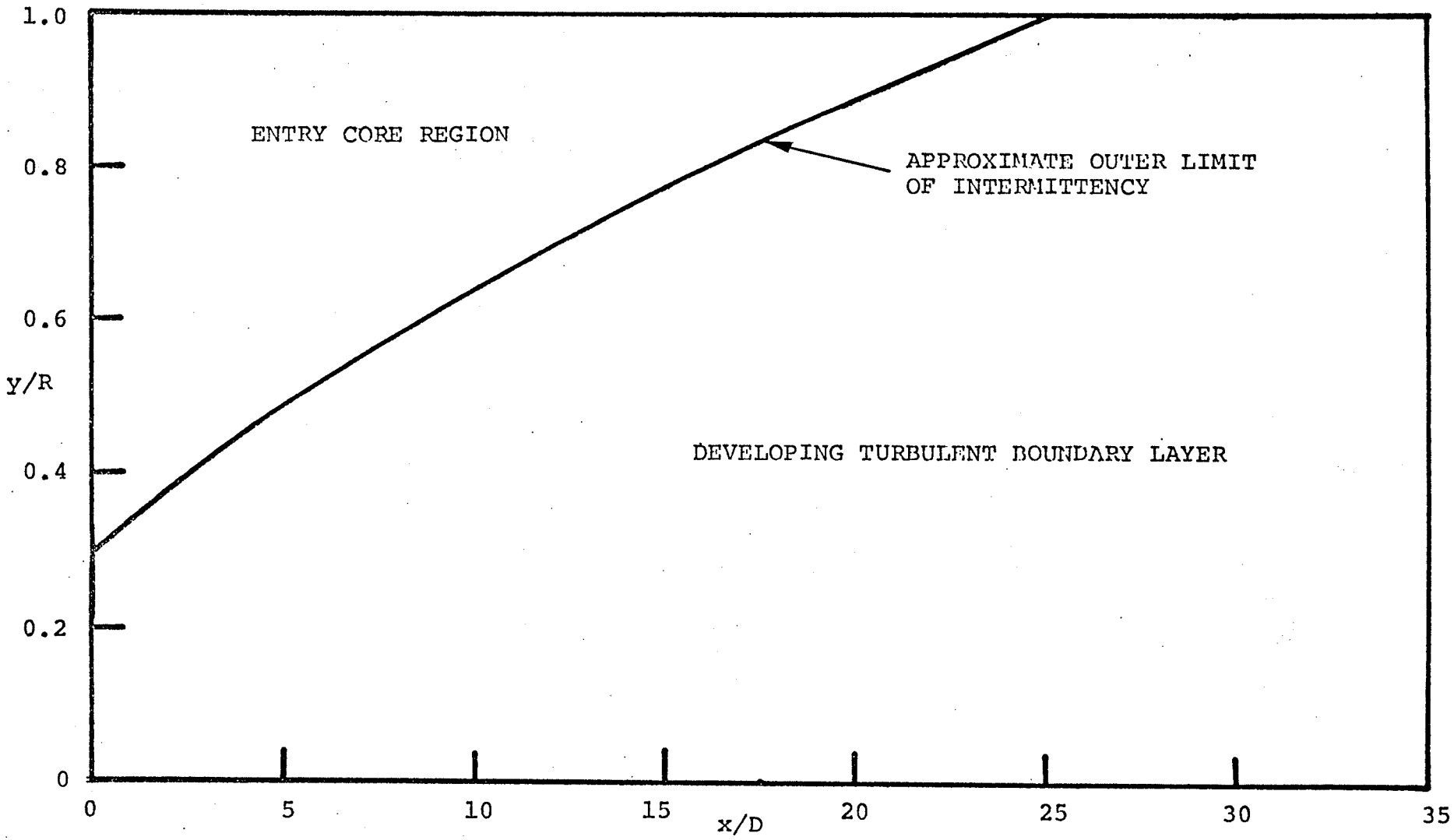

FIGURE 6. Approximate outer limit of intermittency. Re = 3 x 10^5.

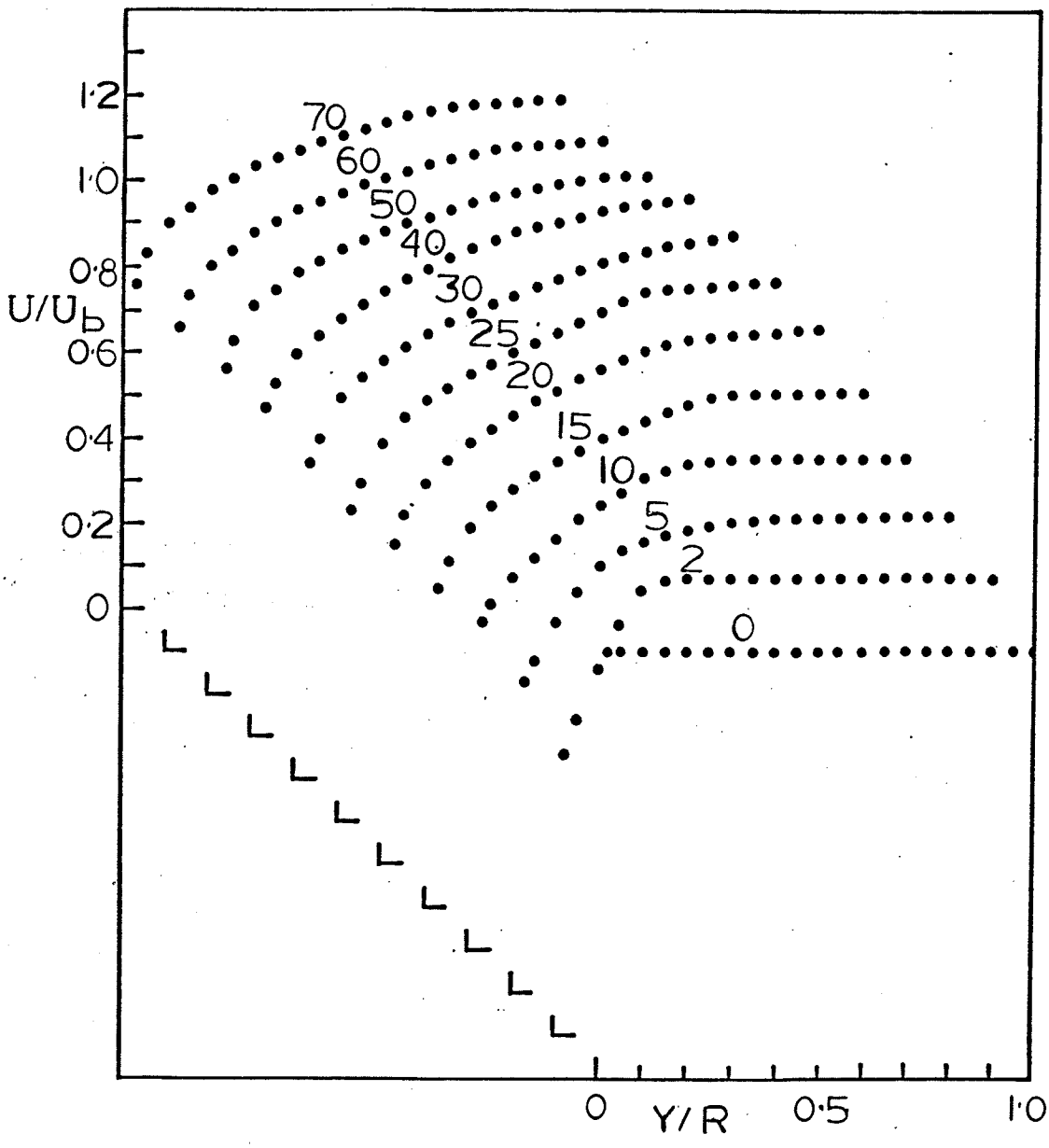

FIGURE 7. Non-dimensionalised axial velocity profiles in developing flow, Re = 3 x 10^5. (Note: each successive profile is displaced by U/U_b = +0.2 and y/R = -0.1 from one another from x/D = 0.)

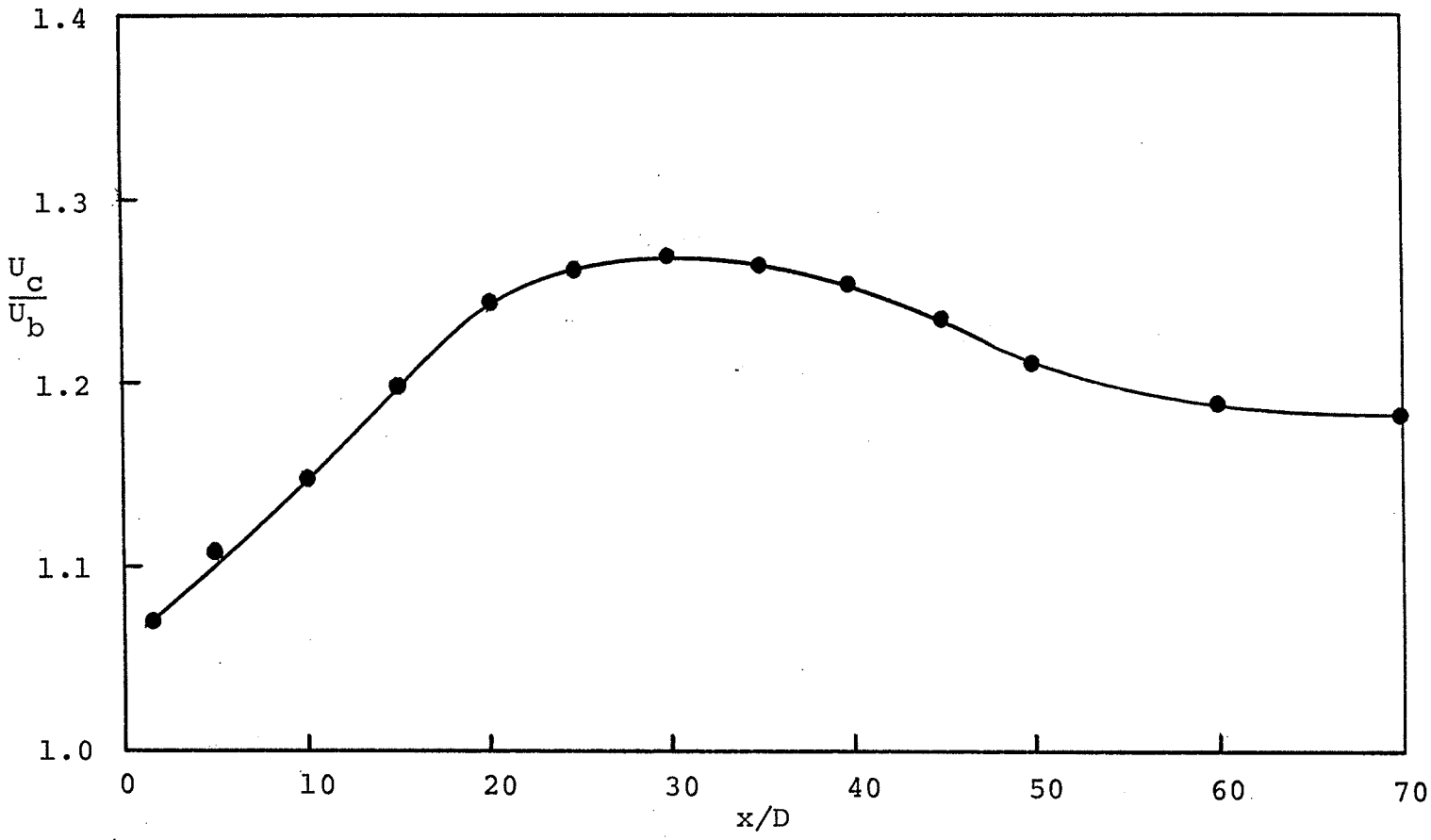

FIGURE 8. Mean centre-line velocity in developing flow, Re = 3 x 10^5.

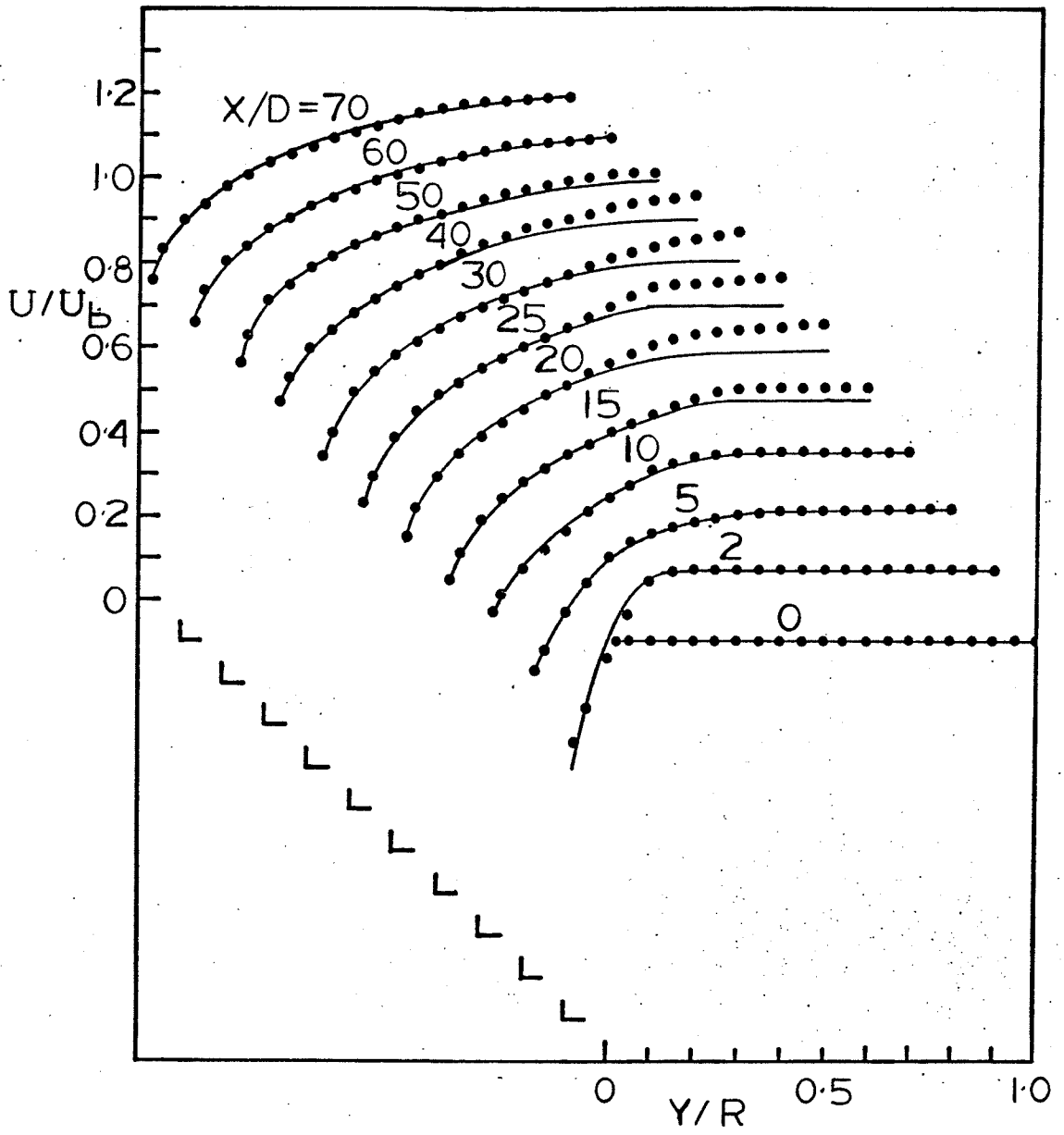

FIGURE 9. Comparison of numerical solution with measured axial velocity profiles, Re = 3 x 10^5. (Note: each successive profile is displaced by U/U_b = +0.2 and y/R = -0.1 from one another from x/D = 0.)

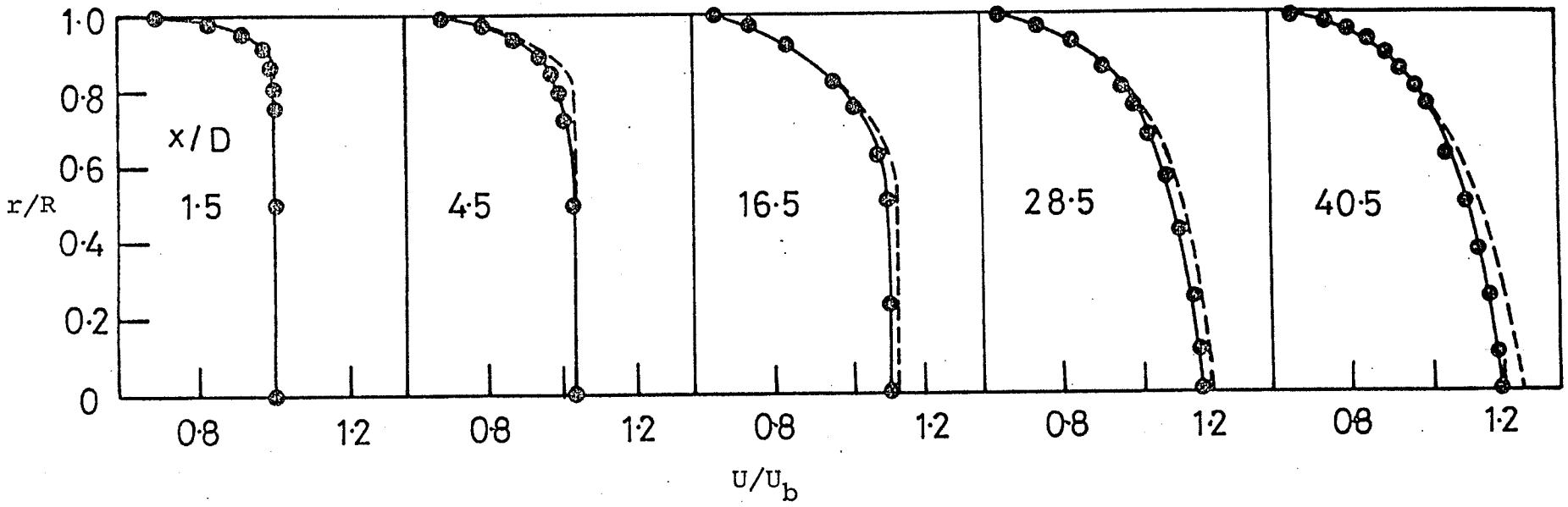

FIGURE 10. Axial velocity profiles in developing flow, Re = 3.88×10^5. —— Numerical solution, ---- Integral solution of Bradley and Cockrell (1970), ● Data of Barbin (1961).

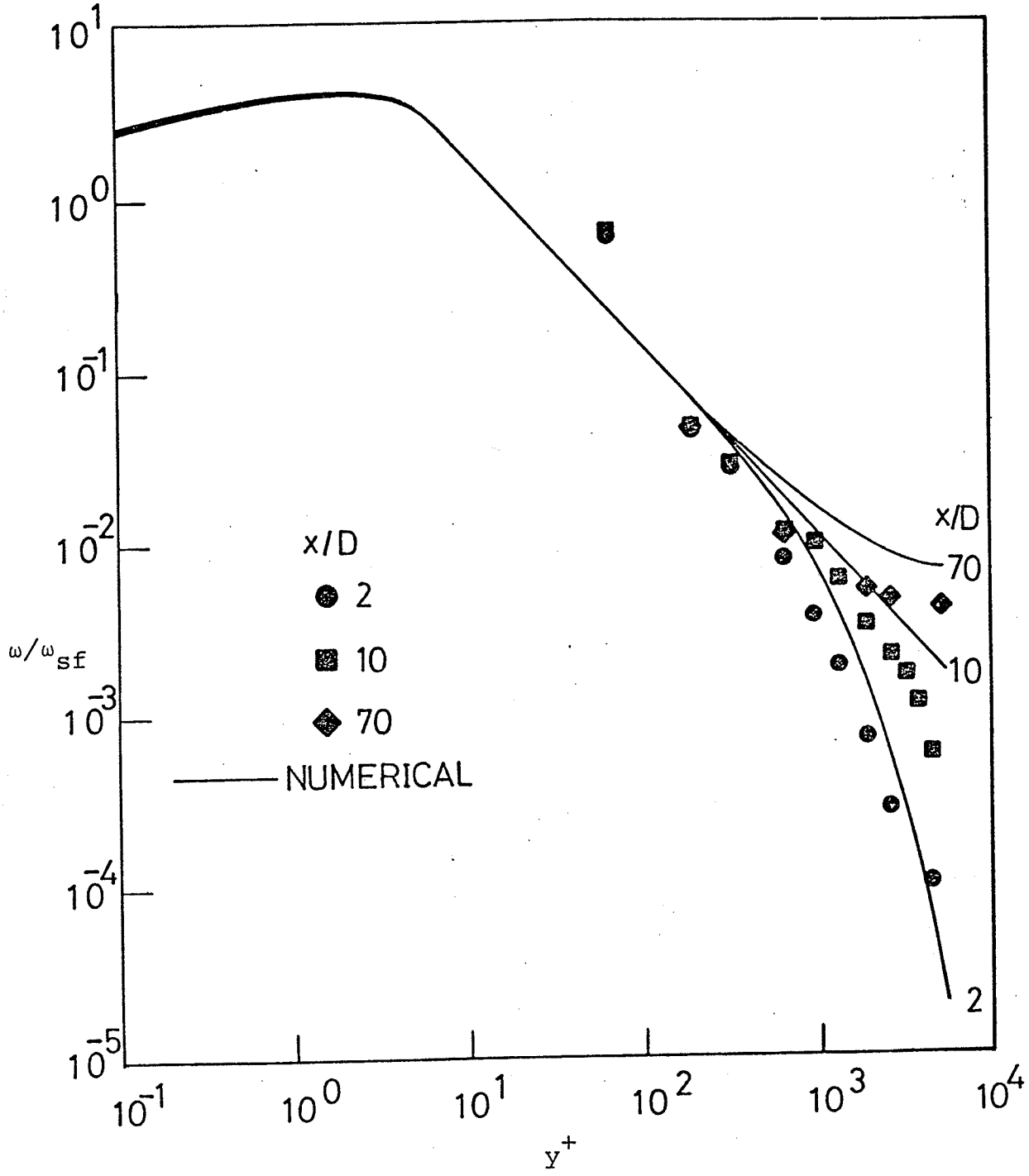

FIGURE 11. Distribution of mean vorticity in developing flow, Re = 3 x 10^5.

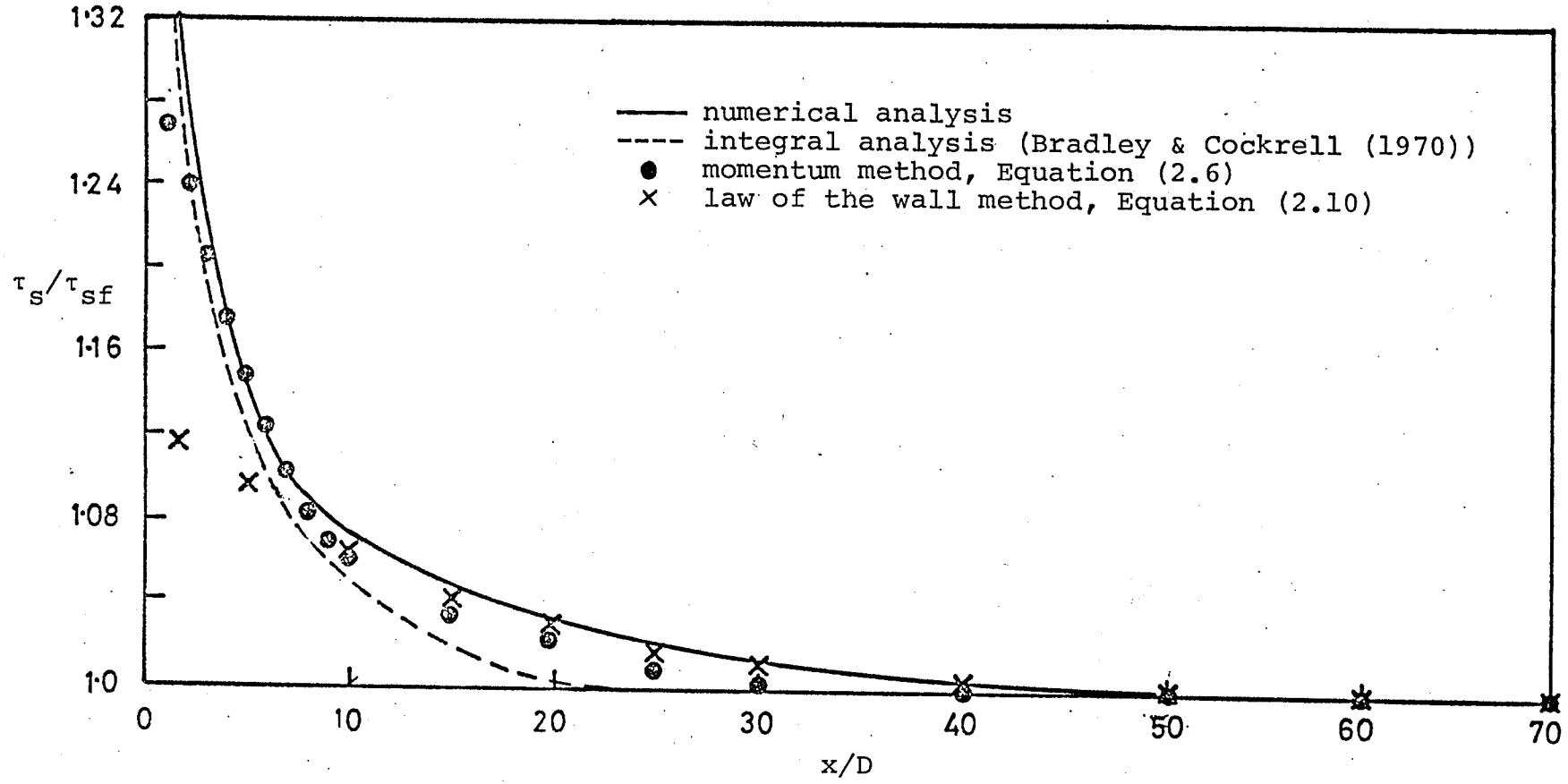

FIGURE 12. Axial development of local wall shear stress, Re = 3 x 10^5.

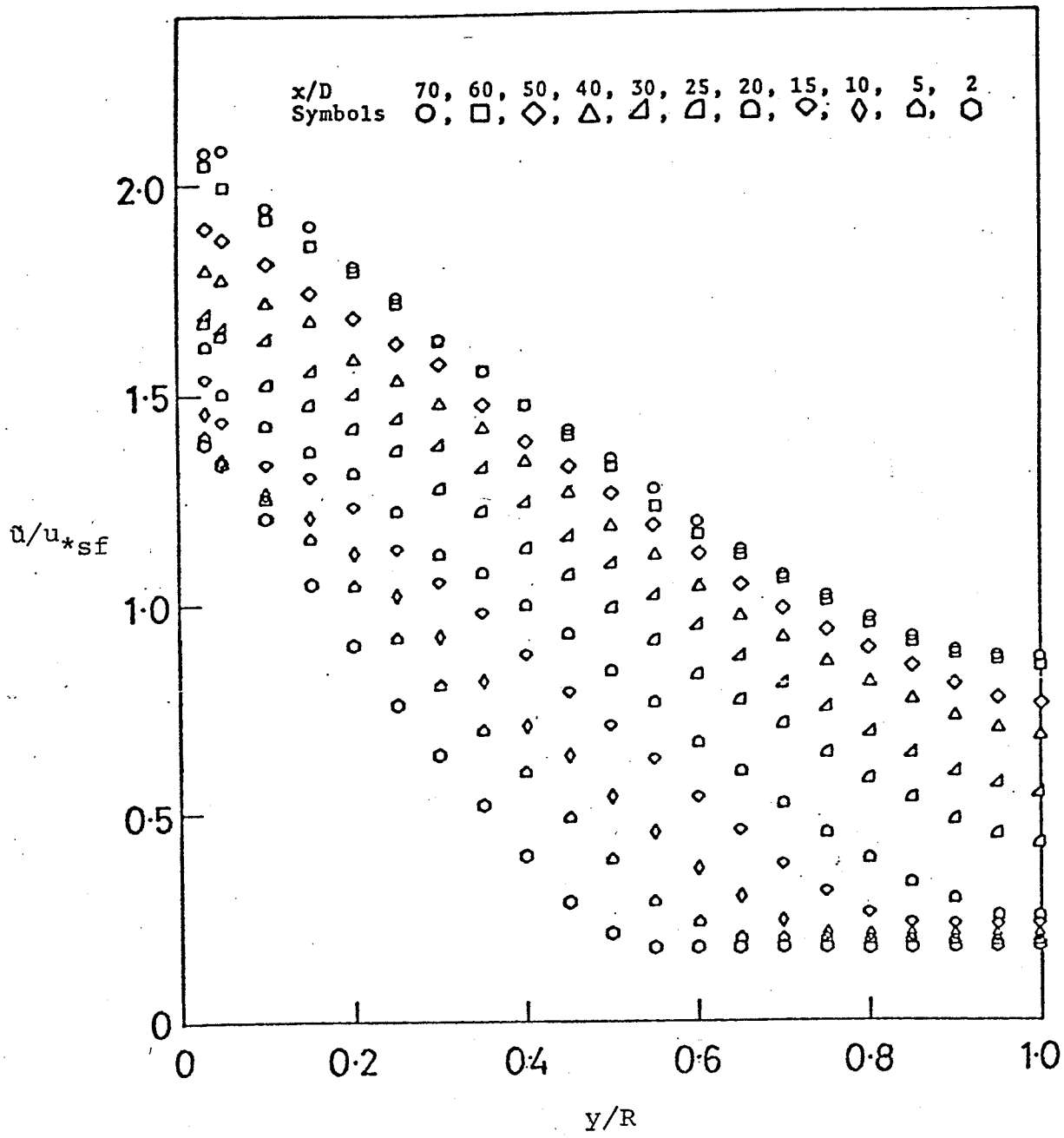

FIGURE 13. Axial fluctuating velocity distribution, Re = 3 x 10^5, single-wire probe.

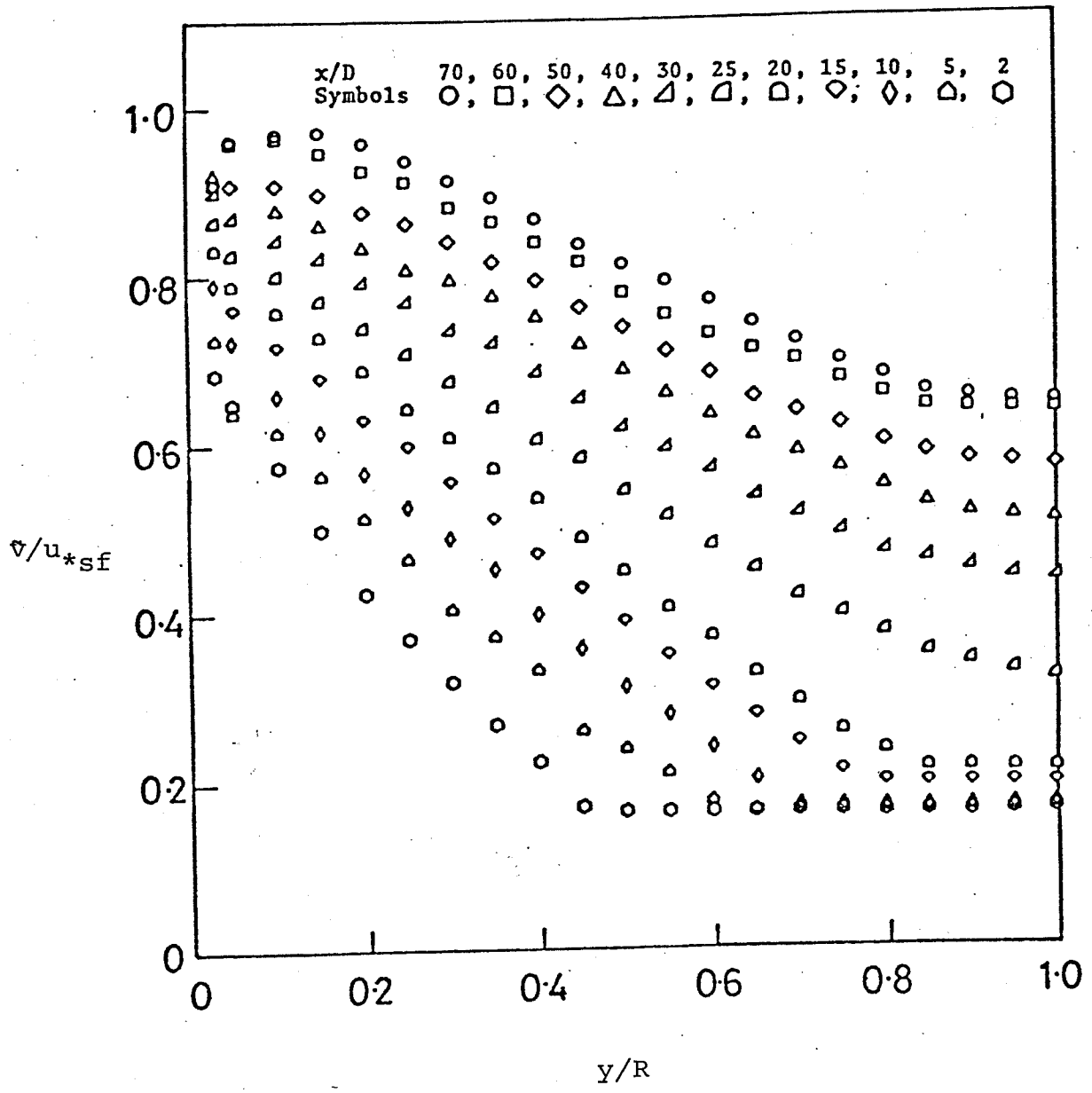

FIGURE 14. Radial fluctuating velocity distribution, Re = 3 x 10^5, x-probe.

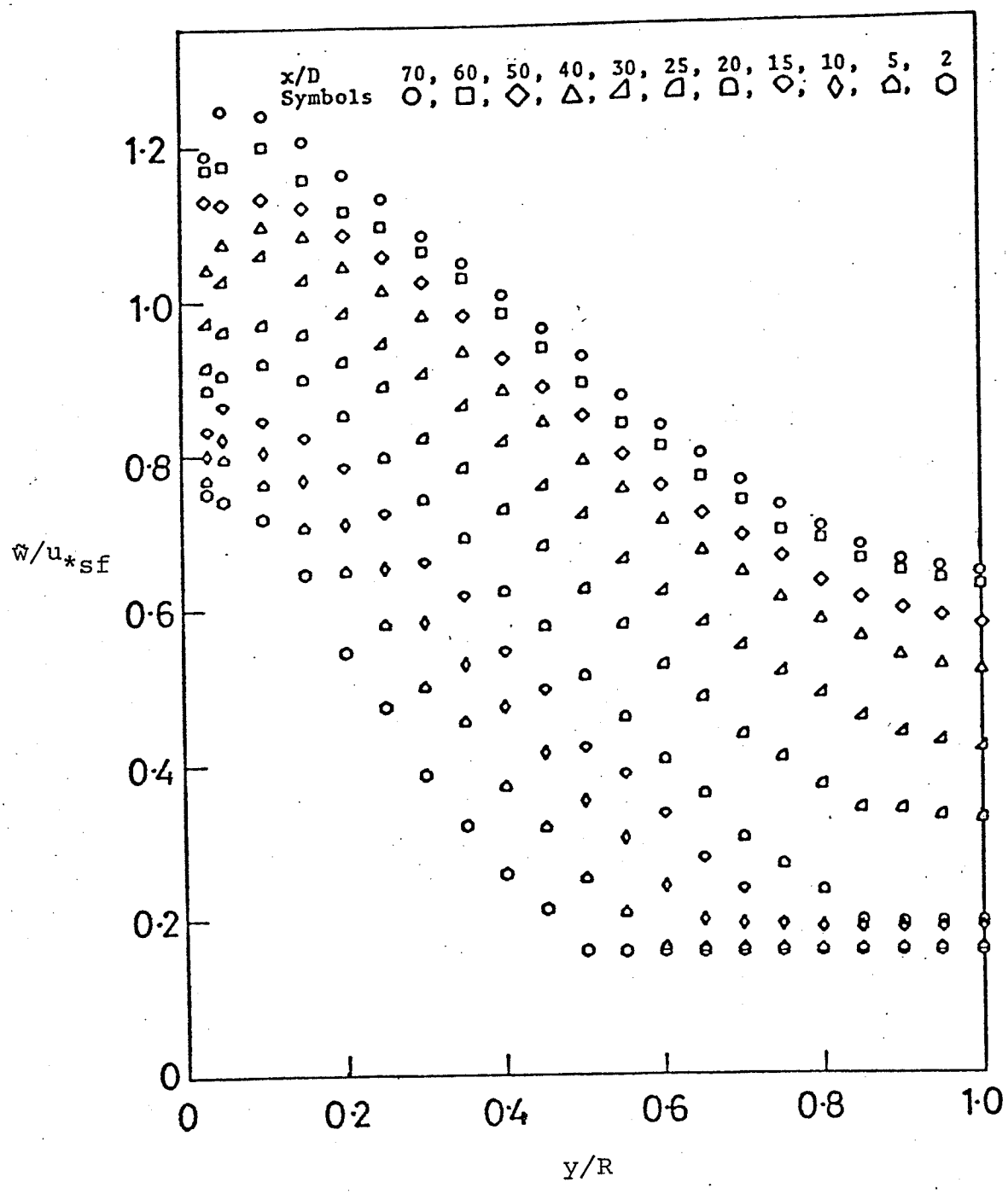

FIGURE 15. Circumferential fluctuating velocity distribution, Re = 3 x 10^5, x-probe.

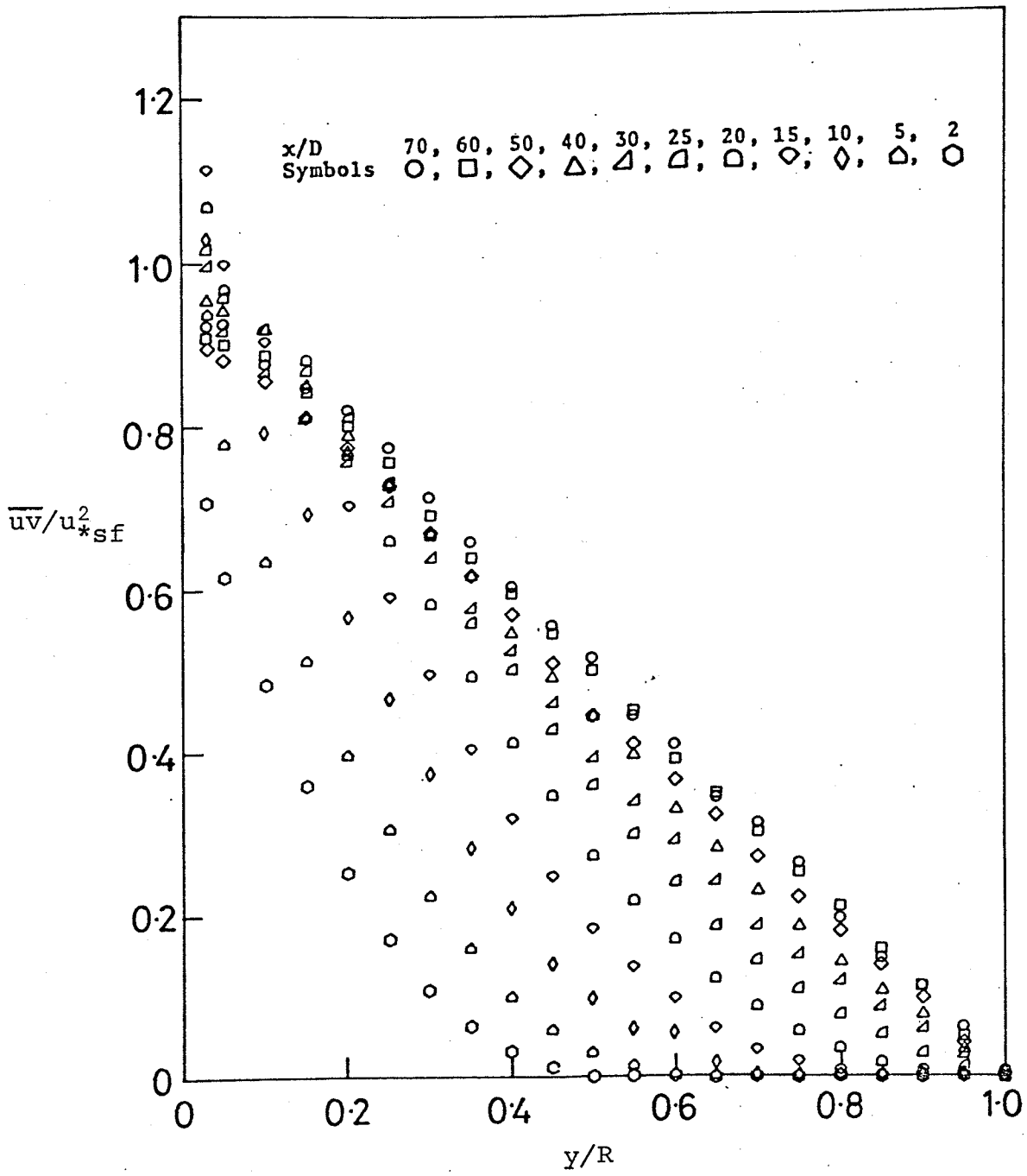

FIGURE 16. Reynolds shear stress distribution in developing flow, Re = 3 x 10^5, x-probe.

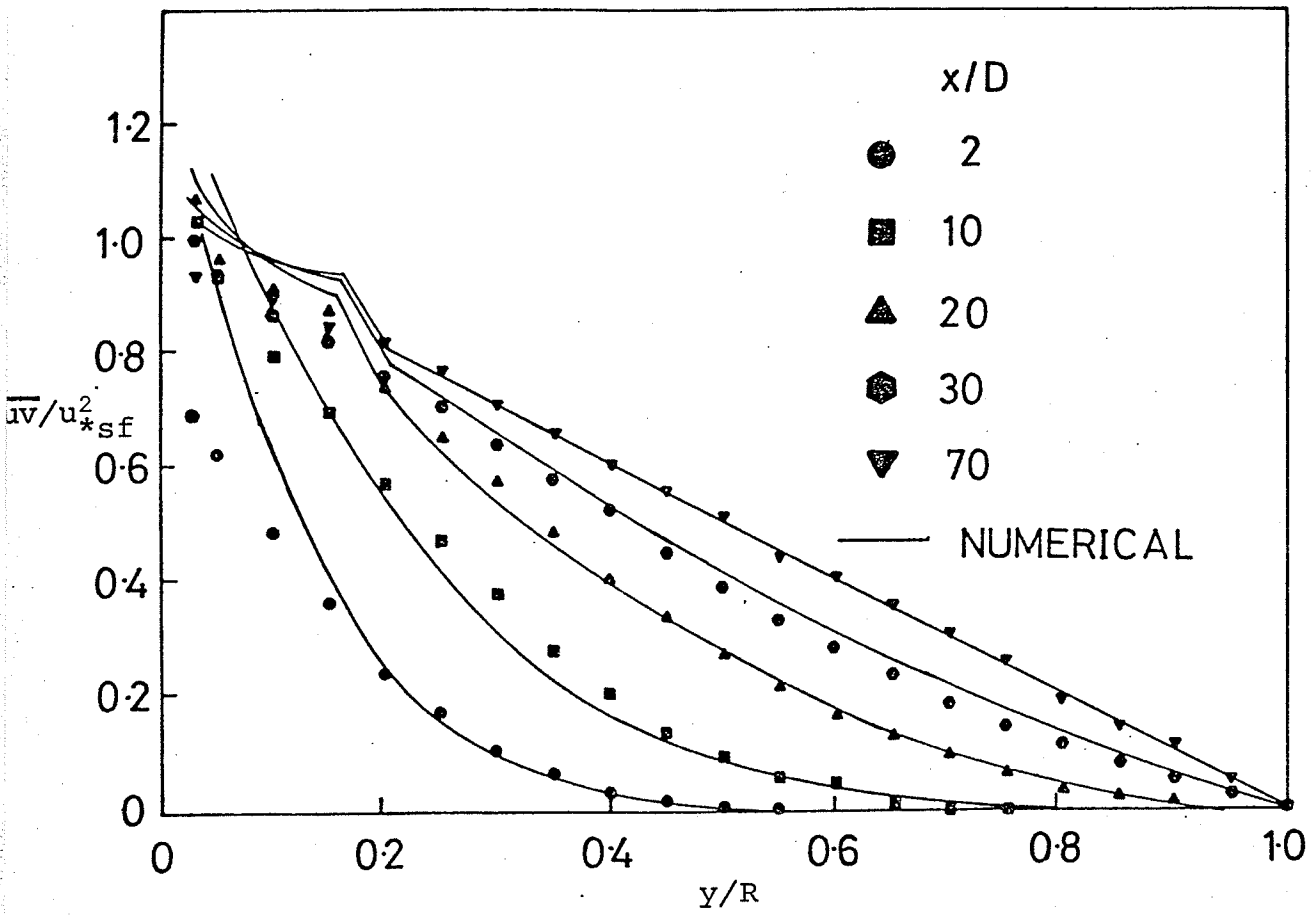

FIGURE 17. Shear stress distributions, Re = 3 x 10^5.

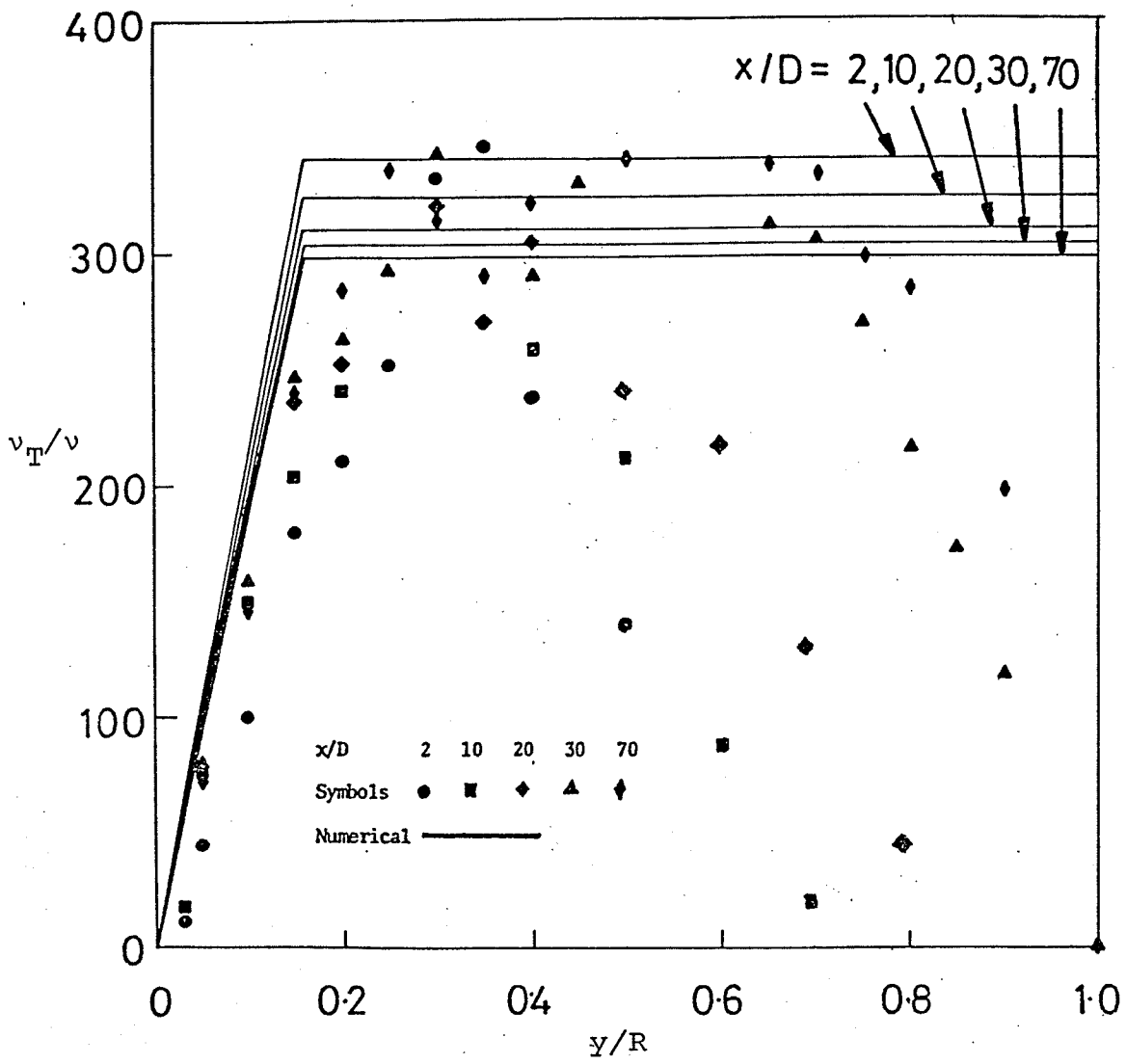

FIGURE 18. Eddy viscosity distribution in developing flow, Re = 3 x 10^5.

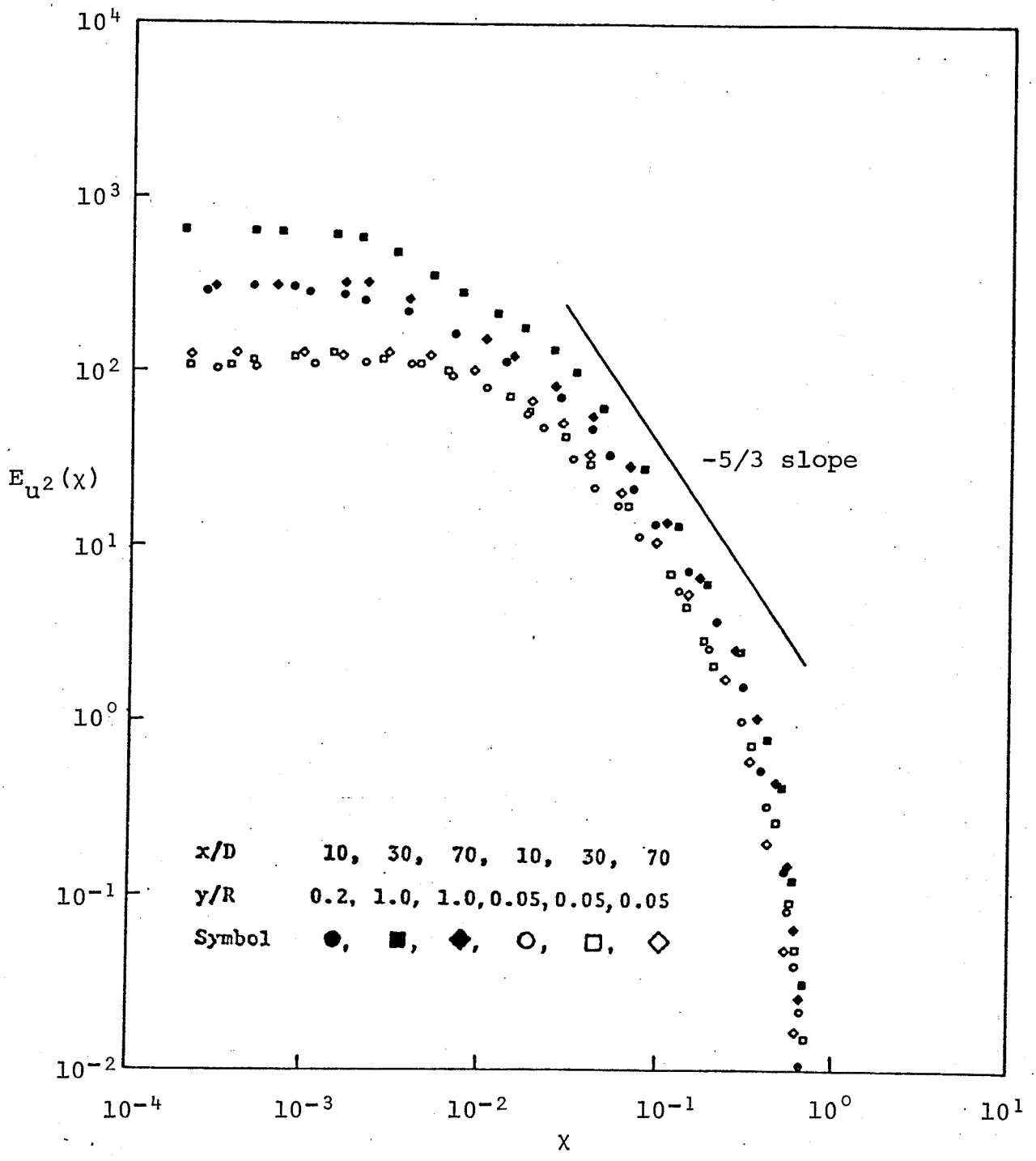

FIGURE 19. Energy spectra - axial component, Re ≅ 3 x 10^5, x-probe.

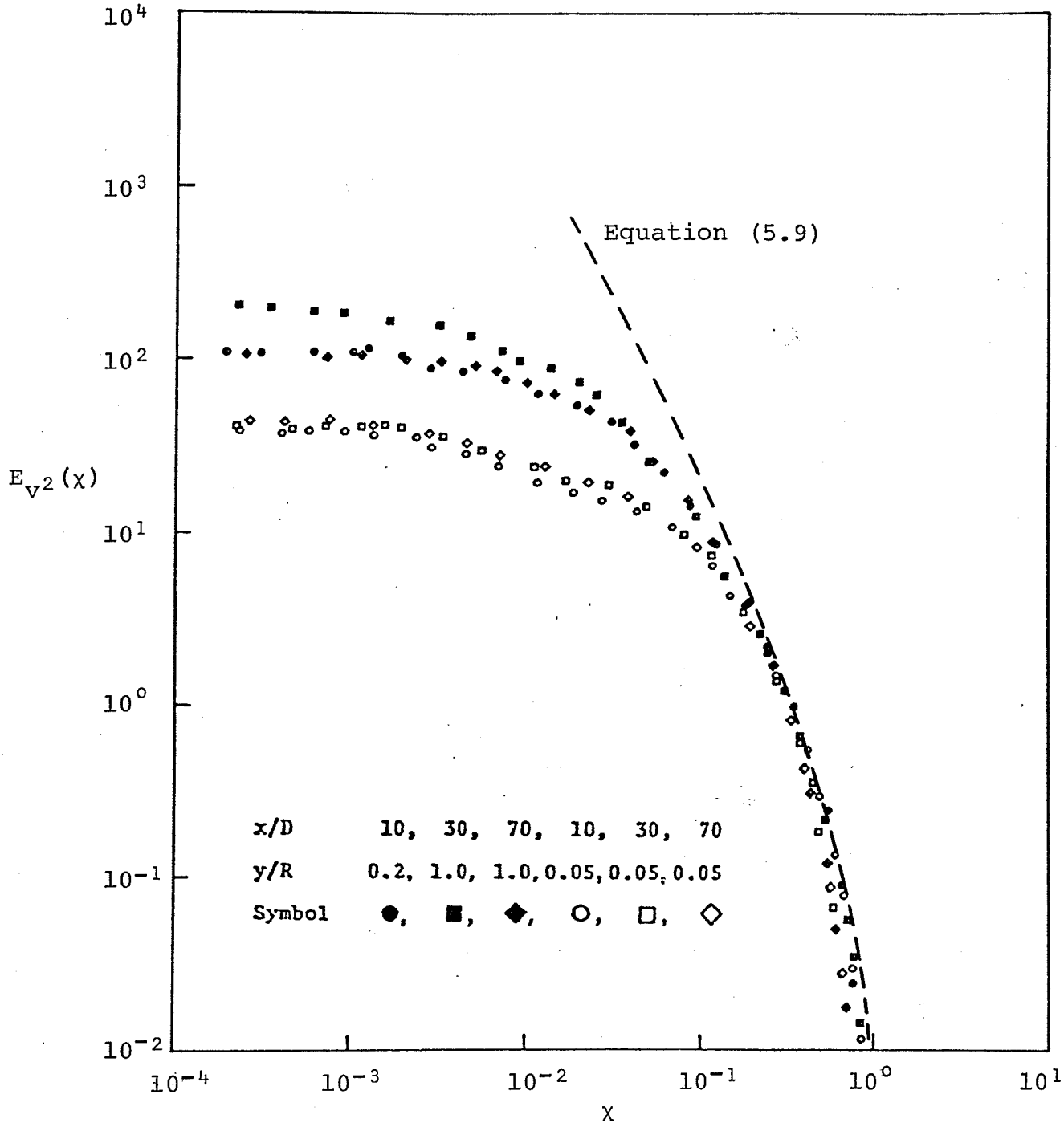

FIGURE 20. Energy spectra - radial component, Re = 3 x 10^5, x-probe.

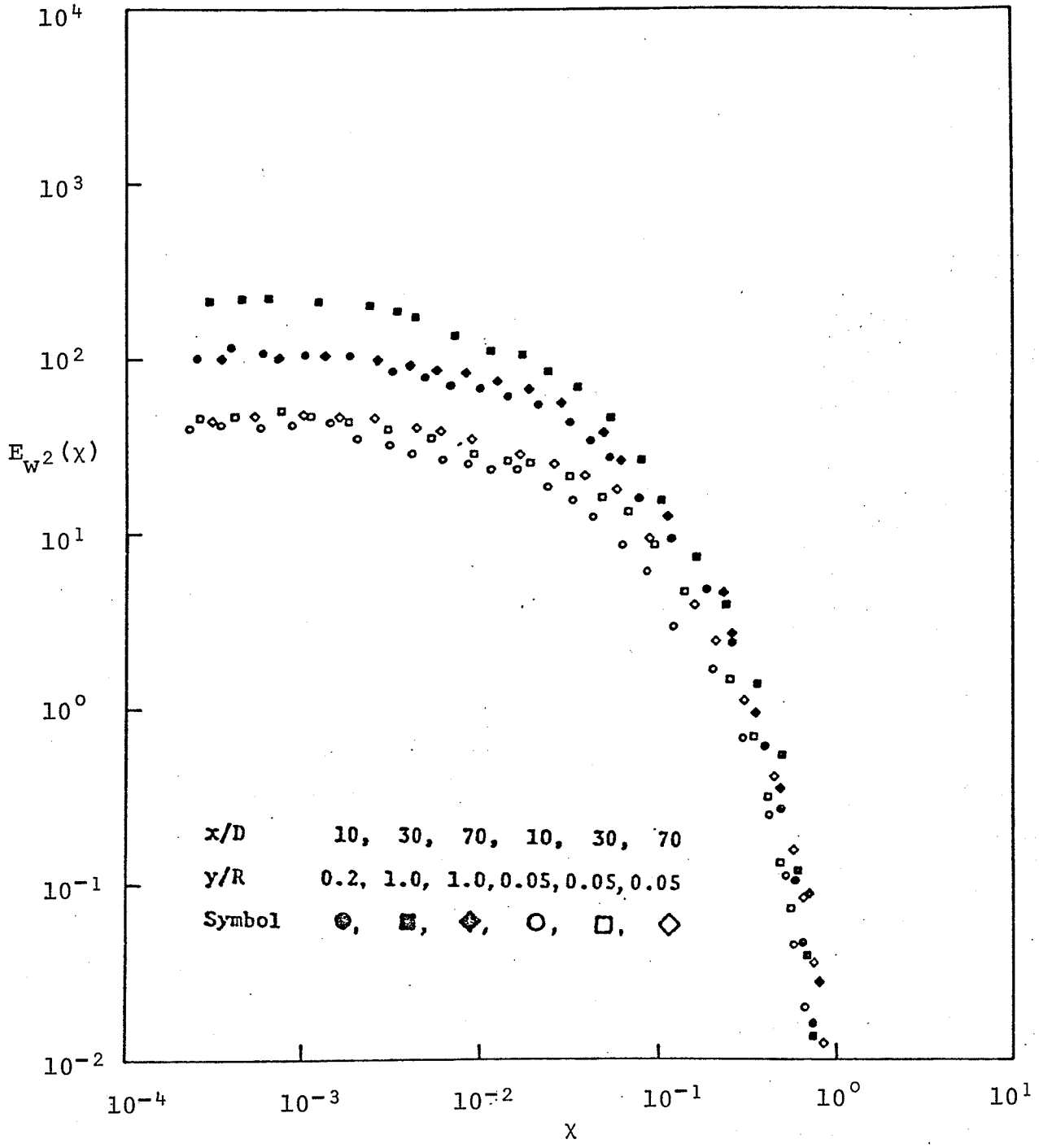

FIGURE 21. Energy spectra - circumferential component, Re = 3 x 10^5, x-probe.

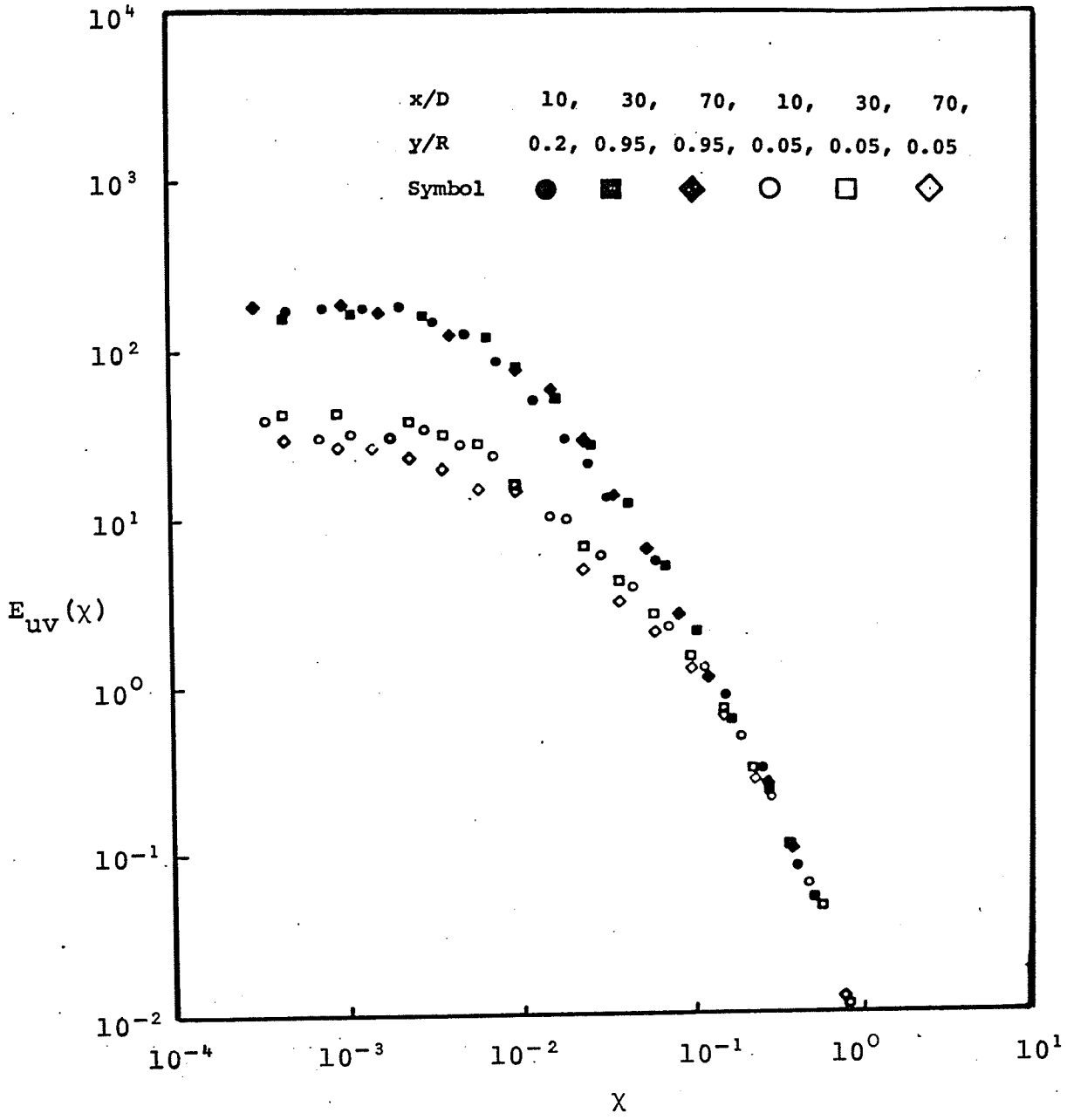

FIGURE 22. Energy spectra - cospectra, Re = 3 x 10^5, x-probe.

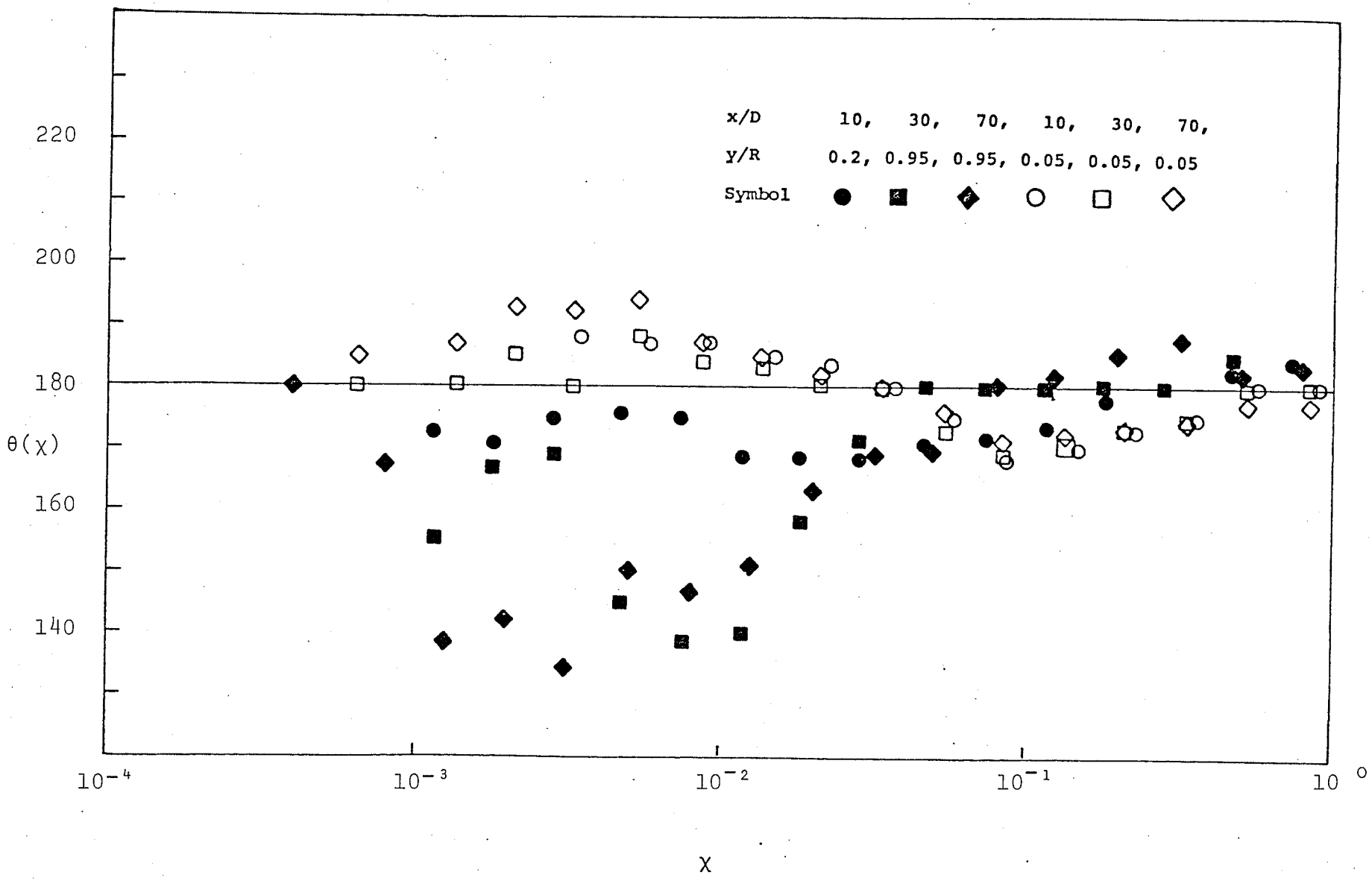

FIGURE 23. Phase-shift, Re = 3 x 10^5, x-probe.

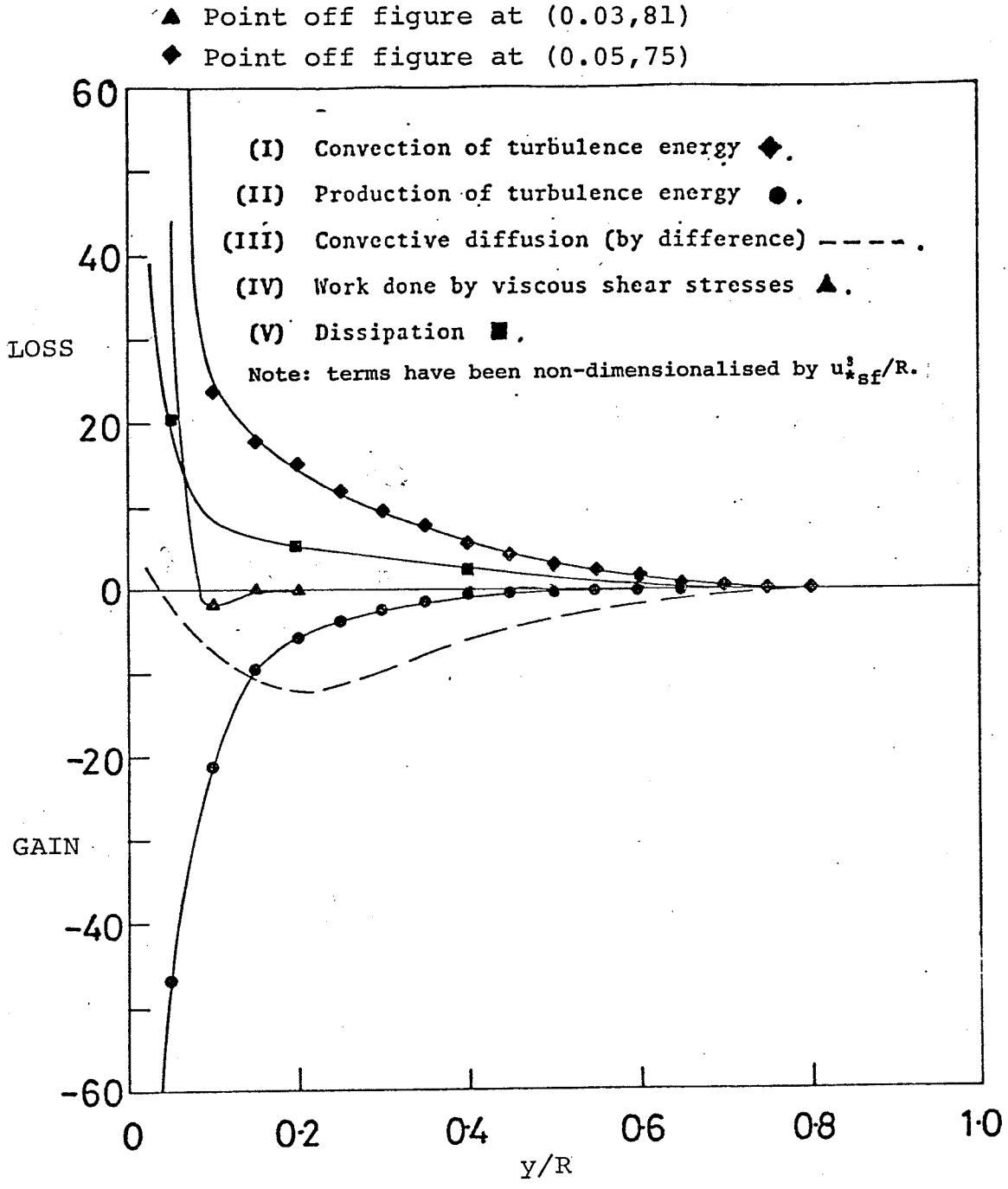

FIGURE 24. Energy balance, Re = 3 x 10^5, x/D = 10.

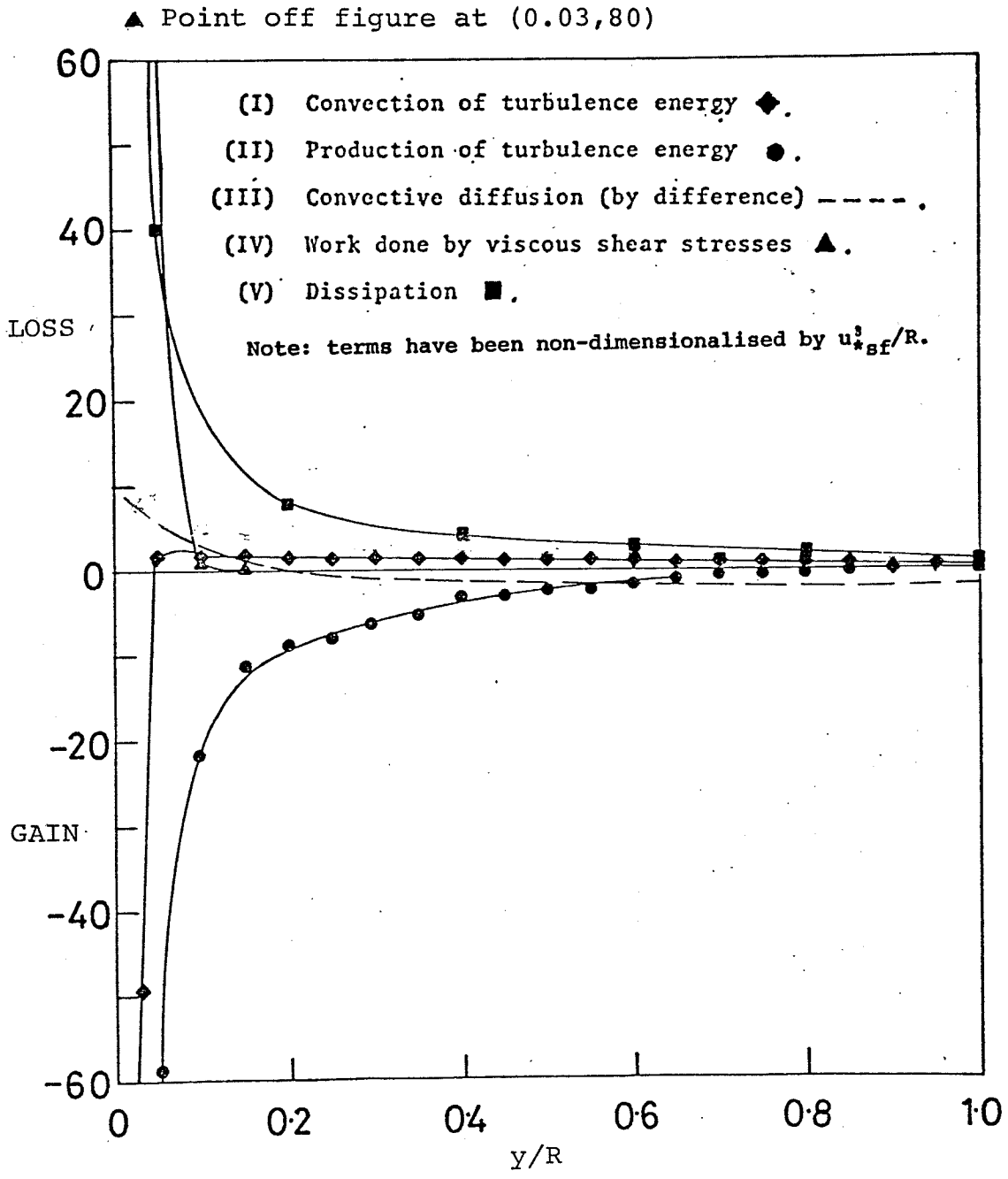

FIGURE 25. Energy balance, Re = 3 x 10^5, x/D = 30.

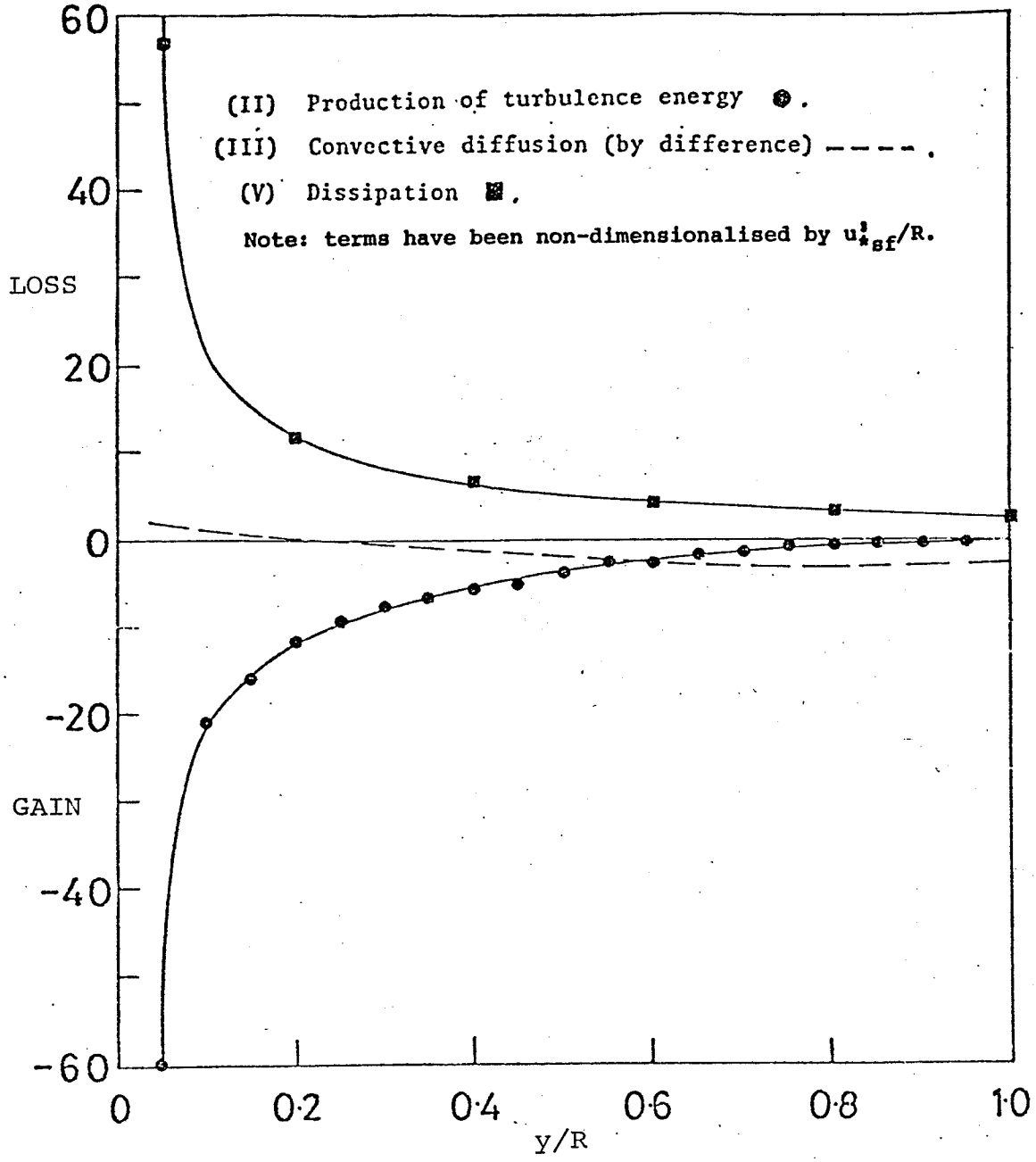

FIGURE 26. Energy balance, Re = 3 x 10^5, x/D = 70.

VITA

JACK WILLIAM RICHMAN

1941 Born, February 20th, at Gillingham, Kent, England.

1953-60 Student, Chatham Technical School for Boys.

1960-63 Kent County Scholar at University College Swansea, University of Wales. Graduated B.Sc. (Honours Physics) 1963.

1963-64 Studied Nuclear Physics at University of Windsor, Ontario, Canada. Funded by University Graduate Fellowship.

1964-66 Aircrew, Royal Canadian Airforce. Rank F/O, Service Number 86458.

1966-68 Senior Engineer, Rocket and Space Division, Bristol Aerospace, Winnipeg, Manitoba. Also part-time student at University of Manitoba. Graduated M.Sc. (Mech. Eng.) 1968.

1968-69 Enrolled in Ph.D. programme in Mechanical Engineering Department, University of Manitoba. Research assistant and lecturer in thermodynamics.

1969-70 Attended low speed aerodynamics course at Von Karman Institute for Fluid Dynamics, Rhode St. Genese, Belgium. Funded by National Research Council of Canada. Graduated V.K.I. Dip. 1970.

1970-73 Resumed study in Ph.D. programme in Mechanical Engineering Department at University of Manitoba, under National Research Council of Canada Scholarship. Engaged in turbulence research and was in instructor in fluid mechanics.

1973 At present employed by Dilworth, Secord, Meagher and Associates, Toronto, under a National Research Council of Canada Industrial Postdoctorate Fellowship.

Activities:

Sailing and tennis.

PUBLICATIONS

RICHMAN, J.W. 1967 Theoretical and experimental results using fiberglass as an ablative material on the Black Brant III nosecone. AIAA Sounding Rocket Vehicle Technology Specialist Conference. Williamsburg, Virginia, U.S.A. February 27 - March 1.

RICHMAN, J.W. 1968 A theory of ablative heat transfer and experimental verification under flight conditions. University of Manitoba. M.Sc. Thesis No. 77044.

RICHMAN, J.W. 1969 Ablative stagnation point heat transfer C.A.S.I. Transactions. Vol 2, No. 1.

RICHMAN, J.W. 1970 Non-stagnation point ablative heat transfer. C.A.S.I. Transactions. Vol 3, No. 2.

RICHMAN, J.W. 1970 An experimental and theoretical study of the interaction between a two-dimensional turbulent jet and the uniform mainstream (military project). Von Karman Institute for Fluid Dynamics. Project Report #70-258.

RICHMAN, J.W. AND AZAD, R.S. 1973 Developing turbulent flow in smooth pipes. Applied Science Research (to be published).

RICHMAN, J.W. AND AZAD, R.S. 1973 Developing turbulent pipe flow. Journal of Fluid Mechanics (to be published).